# Distributed rhythm generators underlie *Caenorhabditis elegans* forward locomotion

Anthony D. Fouad[1], Shelly Teng[1], Julian R. Mark[1], Alice Liu[1], Pilar Alvarez-Illera[1], Hongfei Ji[1], Angelica Du[1], Priya D. Bhirgoo[1], Eli Cornblath[1], Asuka Guan[2], and Christopher Fang-Yen[1,3]

*1. Department of Bioengineering, School of Engineering and Applied Science, University of Pennsylvania, Philadelphia PA 19104, USA*

*2. Lunenfeld-Tanenbaum Research Institute, Mount Sinai Hospital, Toronto, Ontario M5G 1X5, Canada*

*3. Department of Neuroscience, Perelman School of Medicine, University of Pennsylvania, Philadelphia, PA 19104, USA*

## ABSTRACT

Coordinated rhythmic movements are ubiquitous in animal behavior. In many organisms, chains of neural oscillators underlie the generation of these rhythms. In *C. elegans*, locomotor wave generation has been poorly understood; in particular, it is unclear where in the circuit rhythms are generated, and whether there exists more than one such generator. We used optogenetic and ablation experiments to probe the nature of rhythm generation in the locomotor circuit. We found that multiple sections of forward locomotor circuitry are capable of independently generating rhythms. By perturbing different components of the motor circuit, we localize the source of secondary rhythms to cholinergic motor neurons in the midbody. Using rhythmic optogenetic perturbation we demonstrate bidirectional entrainment of oscillations between different body regions. These results show that, as in many other vertebrates and invertebrates, the *C. elegans* motor circuit contains multiple oscillators that coordinate activity to generate behavior.

## INTRODUCTION

Oscillatory neural activity underlies rhythmic animal behaviors such as feeding and locomotion. Rhythm generating units are sometimes functional in isolated spinal cord and invertebrate nerve cord preparations, producing fictive rhythmic motor outputs that resemble *in vivo* patterns (Marder and Calabrese, 1996; Marder et al., 2005; Kiehn, 2006; Mullins et al., 2011; Grillner and El Manira, 2015). At the same time, sensory feedback and reflex loops have also been found to be important for motor rhythm coordination and modulation (Wendler, 1974; Andersson et al., 1981; Yu and Friesen, 2004; Kristan et al., 2005).

How do cellular pacemakers, network oscillators, and sensory feedback interact to perform rhythmic motor generation and coordination? The identification and study of locomotor Central Pattern Generators (CPGs) in the mammalian spinal cord has been complicated by the system's complexity and the large numbers of neurons that are potentially involved. As a result, many components of the mammalian locomotor rhythm generator remain unidentified (Kiehn, 2006; Mullins et al., 2011; Kiehn, 2016). However, work on vertebrate and invertebrate models, such as swimming leeches and lampreys, has allowed the basic principles and components of neural oscillators to be identified (Goulding, 2009; Mullins et al., 2011).

Electrophysiological studies on the leech isolated ventral nerve cord (VNC) have found that individual ganglia distributed along the body can generate oscillatory patterns that mimic those of normal swimming (Weeks, 1981; Kristan et al., 2005; Marder et al., 2005). Stretch sensation and central control couple the oscillatory units in both the ascending and descending directions, such that the intact animal's entire circuit functions in synchrony during swimming (Mullins et al., 2011).

In the lamprey, excitatory interneurons proposed to be rhythm generators are also found throughout the approximately 100 spinal segments, which can generate oscillations when isolated (Mullins et al., 2011; Kiehn, 2016). The distributed nature of rhythm generation in swimming models bears some resemblance to that found in hindlimb locomotion in limbed vertebrates, for which rhythm generating capability is distributed along the caudal spinal cord (Kiehn, 2006). Moreover, analogues of many of the key neuronal classes underlying these behaviors in lampreys and zebrafish are also found in the mouse spinal cord (Goulding, 2009; Kiehn, 2016).

Despite these findings, a clear understanding of how motor systems generate locomotory oscillations at the network, cellular, and molecular levels remains elusive. In both the leech and lamprey, identification of the neurons responsible for rhythm generation remains incomplete, and the mechanism(s) by which these neurons generate swim rhythms are unclear (Kristan et al., 2005; Mullins et al., 2011). In the lamprey, proposed oscillator neurons have not been directly shown to generate the swimming rhythm (Kiehn, 2016). Moreover, the paucity of genetic manipulations available in these organisms makes it difficult to describe molecular mechanisms that contribute to rhythm generation.

The roundworm *C. elegans* is a promising model for achieving an integrated behavioral, circuit, and molecular understanding of how locomotion is generated and coordinated. *C. elegans* has a compact nervous system containing a few hundred neurons, for which a nearly complete wiring diagram of synaptic connectivity has been mapped (White et al., 1986; Varshney et al., 2011). Worms' optical transparency allows researchers to monitor neural activity with genetically encoded calcium and voltage sensors (Kerr et al., 2000; Kerr, 2006; Flytzanis et al., 2014), and manipulate neurons and muscles using optogenetics (Nagel et al., 2005; Zhang et al., 2007; Leifer et al., 2011; Stirman et al., 2011; Husson et al., 2012; Kocabas et al., 2012; Fang-Yen et al., 2015; Gao et al., 2015). *C. elegans* is readily amenable to a powerful set of genetic

manipulations (Ahringer, 2006; Evans, 2006), and shares extensive genetic homology with humans (Lai et al., 2000). Classical neurotransmitters involved in *C. elegans* locomotion include acetylcholine (Rand, 2007), GABA (Jorgensen, 2005), glutamate (Brockie and Maricq, 2006), and the biogenic amines dopamine and serotonin (Chase and Koelle, 2007).

*C. elegans* moves forward by generating sinusoidal dorso-ventral bending waves that propagate from anterior to posterior. The circuit for locomotion consists of interneurons, excitatory and inhibitory motor neurons, and body wall muscles (White et al., 1976; Chalfie et al., 1985; White et al., 1986; Altun and Hall, 2011). The majority of motor neuron cell bodies are located in the ventral nerve cord (VNC), which runs along the ventral side of the body from head to tail (White et al., 1986; Altun and Hall, 2011). The VNC motor neurons include A, B, VC, D, and AS cell types. Laser ablation studies have shown that the A-type neurons are essential for reverse locomotion, whereas the B-type are required for forward locomotion (Chalfie et al., 1985). The D-type (GABAergic) motor neurons are required for a normal amplitude of body bending waves but are not essential for locomotion itself (McIntire et al., 1993b). The function of the AS neurons is unknown. The VC neurons are involved in egg laying (Waggoner et al., 1998). These classes all form neuromuscular junctions with body wall muscles (BWMs).

While the basic architecture of the motor circuitry has been delineated by laser ablation studies, much less is understood about how its components interact to generate coordinated locomotory behavior. Perhaps most notably, it is not known which elements generate the worm's dorso-ventral oscillations during forward movement, nor how many such rhythm generators may exist. Worms are capable of limited movement despite ablation of most premotor interneurons (Chalfie et al., 1985; Wicks and Rankin, 1995; Zheng et al., 1999). When all premotor interneurons are removed, animals did not generate directional movement, but retained the ability to generate local body bends (Kawano et al., 2011). However, forward locomotion was observed after ablation of all premotor interneurons and A motor neurons (Gao et al;

accompanying paper), suggesting that periodic bending during forward locomotion may be organized at the level of the non-A motor neurons and/or the body wall muscles.

Sensory feedback has been shown to play an important role in coordinating *C. elegans* motor behavior. The frequency of *C. elegans* undulation depends continuously on mechanical loading by its environment (Berri et al., 2009; Fang-Yen et al., 2010), and computational models based on proprioceptive feedback and coupling have recapitulated key aspects of locomotory behavior (Boyle et al., 2012; Wen et al., 2012). Experiments in which the worm's body was partially immobilized in a microfluidic device showed that the posterior B-type motor neurons mediate anterior-to-posterior proprioceptive coupling(Wen et al., 2012). B-type motor neurons sense the body curvature and induce bending in the same direction (ventral or dorsal) posterior to the sensed bending.

These findings suggested a model for forward locomotion, similar to one proposed earlier (Karbowski et al., 2008), in which a single rhythm generator generates bending undulations in the head, and these undulations propagate through the body from anterior to posterior via proprioceptive coupling (Wen et al., 2012). This model successfully reproduced the continuous variation in locomotory characteristics observed in varied mechanical environments (Berri et al., 2009; Fang-Yen et al., 2010). This work, while demonstrating how a wave can be propagated along the body, did not directly address the identity of the rhythmic generator(s). Furthermore, it focused on coupling in the posterior of the worm and did not determine whether head and neck proprioception is similarly essential for bending wave propagation.

How might the locomotory circuit be organized? The circuit contains one or more oscillators (**Figure 1**). A model including a single oscillator with proprioceptive coupling (**Figure 1C**) predicts that a disruption in body bending at any location will inhibit posterior bending (**Figure 1E**). Alternative possibilities (Gjorgjieva et al., 2014; Zhen and Samuel, 2015) include the

121 presence of multiple oscillators distributed along the motor circuit (**Figure 1D**), as in the
122 vertebrate spinal cord (Kiehn, 2006; Mullins et al., 2011; Kiehn, 2016) and in the VNC of some
123 invertebrates (Kristan et al., 2005). These oscillatory units could be capable of generating
124 undulations in the posterior of the worm even if anterior neural activity or physical bending is
125 interrupted (**Figure 1F**).

126 In this work, we used spatiotemporally targeted optogenetic illumination (Leifer et al., 2011;
127 Stirman et al., 2011) and lesion studies to show that the mid-body VNC motor circuit contains
128 multiple units capable of independent oscillation. We found a fundamental architecture in the *C.*
129 *elegans* motor circuit similar to that previously described in other vertebrate and invertebrate
130 models.

131

132 **RESULTS**

133 **Rhythmic posterior undulation persists despite anterior paralysis**

134 We first sought to test a model in which there is a single oscillator in the head and
135 proprioceptive feedback is the dominant organizer of bending waves along most of the body
136 (**Figure 1C**). This model, supported by experiments showing that immobilization of the mid-body
137 of worms induced the posterior to adopt the same direction of curvature as the immobilized
138 region (Wen et al., 2012), predicts that paralysis of any region will eliminate undulations
139 posterior to the paralyzed region (**Figure 1E)**. In particular, we asked whether paralysis of the
140 head and "neck" (a region immediately posterior to the head) would halt body bending posterior
141 to these regions.

142 To manipulate neural and muscular activity in freely moving worms, we constructed an
143 optogenetic targeting system similar to that previously described (Leifer et al., 2011). Briefly, this

144 system uses real-time imaging processing and a digital micromirror device to project laser
145 illumination onto arbitrarily specified regions of an unrestrained worm.

146 To examine the effect of inhibiting anterior muscles, we first used this system to project 532 nm
147 illumination onto worms expressing the inhibitory opsin halorhodopsin (NpHR/Halo) in all body
148 wall muscles under the control of the *myo-3* promoter (Zhang et al., 2007; Leifer et al., 2011).
149 We quantified the movement of worms before and during optogenetic manipulation by
150 measuring the curvature of the worm over time (**Figure 1 A, B**) (Pierce-Shimomura et al., 2008;
151 Fang-Yen et al., 2010; Leifer et al., 2011; Wen et al., 2012). We specify longitudinal positions
152 via a body coordinate ranging from 0 at the tip of the head to 100 at the end of the tail.

153 Illuminating body coordinates 50-65 in P*myo-3::NpHR* worms caused substantial paralysis in
154 the tail (not shown), consistent with previous findings (Leifer et al., 2011; Wen et al., 2012).
155 When we paralyzed the anterior 33% or 45% of the worm, however, we observed robust
156 oscillations in posterior regions of the body. In addition, we found to our surprise that
157 illumination of the anterior 33% of the body caused the tail's undulation frequency to increase
158 (**Figure 2A, D; Video 1**).

159 Next, we asked whether oscillations in the posterior would persist under optogenetic inhibition of
160 excitatory motor neurons instead of inhibition of muscles. We illuminated worms expressing
161 NpHR in all cholinergic neurons (P*unc-17::NpHR*), including the A-type and B-type motor
162 neurons, head motor neurons, and several other neuronal cell types (Duerr et al., 2008). We
163 found that while optogenetic inhibition of cholinergic neurons in the head and neck caused
164 anterior paralysis, tail undulation often persisted (**Figure 2B, D, Video 1**).

165 During optogenetic muscle or neuron inactivation, the amplitude of the bending wave in the
166 head decreased greatly but did not vanish (**Figure 2A, B, E**), leaving open the possibility that a

residual small amplitude wave allows propagation of the bending wave through the partially paralyzed region. We therefore sought means of paralyzing the head more effectively.

We hypothesized that regional paralysis could be induced by lesioning the anterior BWMs instead of hyperpolarizing them. To selectively lesion muscles, we used region-targeted illumination at 470 nm of P*myo-3::PH::miniSOG* worms in which the photosensitizing protein miniSOG is expressed in body wall muscles (Xu and Chisholm, 2016). The anterior portion of most treated animals was nearly immobile (**Figure 2C, Video 1**, especially the last 8 seconds). Nevertheless, undulation posterior to the region of illumination was routinely observed in these animals.

We also conducted thermal lesioning experiments in which touched the anterior half of the worm with a hot platinum wire attached to a soldering iron. After this treatment, the animal's head and neck were again nearly motionless, yet rhythmic undulation routinely persisted in the tail (**Figure 2 - Figure Supplement 1, Video 1**).

Our finding that posterior undulation can persist despite anterior paralysis is consistent with a multi-oscillator model (**Figure 1D**) and not with a single oscillator model that relies on reflex-like signaling for wave propagation (**Figure 1C**).

**The head and tail are capable of simultaneous oscillations at different frequencies**

The finding that optogenetic inhibition of anterior muscles induces higher frequency oscillations in the tail suggests that an interruption of propagating activity in the motor circuit enables independent activity in a posterior oscillator. To test this idea further, we applied several optogenetic manipulations to inhibit motor coupling in the neck only, leaving the head and tail free to oscillate.

190 First, we optogenetically inhibited neck muscles in P*myo-3::NpHR* worms. In most trials,
191 optogenetically inhibiting neck muscles prevented waves generated in the head from
192 propagating through the neck. During the interruption of these waves the tail exhibited bending
193 undulations at a higher frequency than that of the head, resulting in the animal simultaneously
194 undulating at two distinct frequencies (**Figure 3A, Video 2**). We henceforth refer to this
195 behavior, whether or not induced by any manipulation, as two-frequency undulation (2FU).

196 We observed 2FU upon inhibiting all neck cholinergic neurons (**Figure 3B, Video 2**) and also
197 upon inhibiting neck B-type motor neurons (P*acr-5::Arch*; **Figure 3C, Video 2**). These
198 manipulations did lead to a large decrease in wave amplitude in the neck and a smaller
199 decrease in wave amplitude in the tail (**Figure 3F**). Nevertheless, multiple animals in each
200 experiment showed 2FU, with the highest ratios of tail frequency to head frequency seen in
201 worms in which the neck muscles were inhibited (**Figure 3E**).

202 In some experiments, the optogenetic manipulation of motor neurons or muscles did not
203 completely block wave transmission through the paralyzed region. In these trials, some tail
204 waves appeared synchronized with head waves, whereas others did not (**Figure 3C**). To test
205 whether 2FU can occur after stronger disruption of motor coupling, we lesioned mid-body
206 muscles in P*myo-3::PH::miniSOG* worms. This manipulation indeed led to stronger decoupling
207 between head and tail oscillations, but did still not prevent 2FU (**Figure 3D, Video 2**).

208 If the posterior motor circuit of B and AS type neurons contains additional oscillating units, we
209 reasoned that localized undulations might occur after selectively activating small portions of the
210 motor circuit while inhibiting the rest. We therefore examined worms in which both the inhibitory
211 opsin NpHR and the excitatory opsin Channelrhodopsin-2 (ChR2) were expressed in the
212 cholinergic neurons, after the A-type motor neurons were ablated by P*unc-4::miniSOG*.

213 We first illuminated these animals with 590 nm wavelength (yellow) light throughout the body to
214 inhibit all cholinergic neurons. While maintaining this yellow illumination, we targeted small
215 portions of the tail with 473 nm wavelength (blue) light, activating ChR2 and stimulating a few
216 posterior B and AS neurons. Under these conditions, several animals generated high frequency
217 localized undulations in the tail (**Figure 3 - Figure Supplement 1A, Video 3**). These findings
218 further support the presence of additional oscillator(s) in this region.

219 If multiple independent oscillators underlie a worm's forward movement under physiological
220 conditions, we reasoned that independent head and tail oscillations might also be observable in
221 animals without induced lesions or optogenetic perturbations.

222 Wave frequency depends strongly on the degree of mechanical loading from the environment,
223 for example decreasing with viscosity of the fluid medium (Berri et al., 2009; Fang-Yen et al.,
224 2010). We hypothesized that head and tail oscillations might be decoupled by placing the
225 anterior and posterior of a worm in fluids of different viscosities. When we studied worms
226 transitioning between regions of a low viscosity buffer into highly viscoelastic
227 hydroxypropylmethylcellulose (HPMC) islands (see Methods), we observed 2FU in 6 of 41
228 worms (15%). In these animals, the tail continued oscillating at a high frequency for at least two
229 full cycles even as the head frequency was sharply reduced (**Figure 3 - Figure Supplement**
230 **1B, Video 3**). Although these events were uncommon, they demonstrated that 2FU can occur
231 in *C. elegans* with no internal perturbations.

232 Taken together, these results strongly suggest that the *C. elegans* forward motor circuit contains
233 at least two units capable of independent rhythm generation, and that a partial breakdown in
234 anterior proprioceptive coupling (for example by inhibiting neck BWMs) is sufficient to reveal the
235 presence of the posterior oscillating unit(s).

236

237 **Premotor interneurons are not essential for rudimentary forward movement or 2FU**

238 To better understand the source of tail oscillations during 2FU, we used genetic analysis and
239 lesion studies to ask which components of the motor circuit are required for this behavior.
240 Almost all chemical or electrical synaptic connections to the VNC motor neurons are made by
241 the premotor interneuron (IN) classes AVB, PVC, AVA, AVD, and AVE (White et al., 1986).
242 Laser ablation studies have indicated that AVB, and to a lesser degree PVC, are essential for
243 normal forward locomotion (Chalfie et al., 1985), although rudimentary forward crawling is
244 possible in their absence (Gao et al., 2017). Therefore, we asked whether 2FU is possible in the
245 absence of AVB, PVC, and all other premotor INs.

246 To determine if the premotor interneurons are required for 2FU, we first asked whether
247 optogenetic muscle inhibition in the neck in worms lacking premotor interneurons would induce
248 2FU (**Figure 3A, E**). We used transgenic strains in which expression of the apoptosis-promoting
249 interleukin-converting enzyme (ICE) was used to ablate premotor INs and some other neurons
250 (Zheng et al., 1999). When ICE is expressed under the control of the *nmr-1* or *glr-1* promoters,
251 the PVC, AVA, AVD, and AVE interneurons are removed. AVB, however, are present in both
252 *Pnmr-1::ICE* (Kawano et al., 2011), and P*glr-1::ICE* worms (Kawano, Po, and Zhen, personal
253 communication). We generated the strains P*myo-3::NpHR*; P*glr-1::ICE* and P*myo-3::NpHR*;
254 P*nmr-1::ICE*. We found that both strains were capable of 2FU during optogenetic inhibition of
255 neck muscles (**Figure 4A, E, Figure 4 Figure Supplement 1A, E**). This result demonstrates
256 that 2FU does not require most premotor interneurons, including the forward locomotory
257 interneurons neurons PVC.

258 The interneuron AVB is coupled to the B-type motor neurons by an extensive network of gap
259 junctions. Formation of these connections, as well as electrical coupling between the premotor
260 interneurons and the motor neurons of the circuit for reverse locomotion, requires UNC-7

261 expression in AVB and UNC-9 expression in the B-type motor neurons (Starich et al., 2009;
262 Kawano et al., 2011; Liu et al., 2017). UNC-9 also participates in electrical coupling between
263 BWM cells (Liu et al., 2006). We asked whether animals lacking UNC-7 or UNC-9 could exhibit
264 2FU. We crossed *unc-7* and *unc-9* mutations into our P*myo-3::NpHR* strain and performed
265 optogenetic experiments as before. The *unc-7* and *unc-9* worms are uncoordinated and exhibit
266 significantly reduced spontaneous forward locomotion (Starich et al., 2009; Kawano et al.,
267 2011). To initiate a short bout of forward locomotion, we used a cell phone motor to apply a
268 mechanical stimulus in the form of a 3-5 s, ≈200 Hz vibration of the slide just before illumination.
269 We found that both strains were capable of 2FU, although it appeared to occur less often than in
270 PVC-ablated animals, and sometimes occurred prior to neck muscle inhibition (**Figure 4B, E;**
271 **Figure 4 Figure Supplement 1E; Figure 4 Figure Supplement 5A,B**). This finding shows that
272 the UNC-7/UNC-9 gap junctions, including those between AVB and the B-type motor neurons,
273 are not required for 2FU.

274 Finally, we ablated AVB, labeled by P*sra-11::D3cpv* (Kawano et al., 2011), using a pulsed
275 infrared laser ablation system (Churgin et al., 2013) that we modified to intentionally lesion
276 tissue (see Methods). This procedure generally removed both AVB cell bodies and their
277 associated processes, and possibly other head neurons, but not PVC. When subjected to the
278 same experiment as described above, 2FU events were nearly diminished. Very rarely we
279 observed uncoupled undulation events that were not correlated with neck muscle inhibition
280 **(Figure 4 Figure Supplements 1B, 1E, 2, 5C)**. Taken together, these results suggest that
281 individual classes of premotor interneurons, including AVB and PVC, are not essential for 2FU.
282 However, AVB may play a key role in activating the rhythm generator(s) to allow oscillation.

283

284

285 **Several classes of motor neurons are not required for forward locomotion or 2FU**

286 The premotor interneurons comprise the primary circuit connection between the VNC motor
287 neurons and the worm's other sensory and interneuronal circuits (White et al., 1986). The
288 finding that premotor interneurons are not necessary for forward locomotion and 2FU suggests
289 that high frequency tail undulations during 2FU may originate from the motor neurons
290 themselves. We asked, in the presence of all premotor interneurons, whether any classes of
291 motor neurons are required for 2FU.

292 We first examined the A-type motor neurons. While the A class motor neurons are preferentially
293 active during reverse locomotion (Haspel et al., 2010; Kawano et al., 2011), and are required for
294 reverse locomotion (Chalfie et al., 1985), it is conceivable that they play a role in 2FU. We found
295 that ablating the A- and VC-type motor neurons with a genetically targeted ROS generator
296 (P*unc-4::miniSOG*) did not prevent 2FU induced by neck paralysis during forward locomotion
297 (**Figure 4 - Figure Supplement 1C, E**). This result supports the idea that the A and VC motor
298 neurons are not necessary for the posterior forward oscillator(s).

299 Next, we examined whether the GABAergic D-type motor neurons are required for 2FU. The D-
300 type motor neurons release GABA onto the UNC-49 receptor to trigger contralateral muscle
301 inhibition during a bend. Therefore, the putative null allele *unc-49(e407)* (Bamber et al., 1999;
302 Liewald et al., 2008), should effectively block the functional output of D-type motor neurons.
303 Indeed, *unc-49* mutants exhibited simultaneous dorsal and ventral contractions when stimulated
304 for forward and reversal movement, as did animals in which D motor neurons were ablated
305 (McIntire et al., 1993a). We found that animals harboring an *unc-49(e407)* mutation, while very
306 slow swimmers, were nonetheless capable of 2FU during neck muscle paralysis (**Figure 4D, E**).
307 In one case we observed 2FU before inhibition of neck muscles (**Figure 4 Figure Supplement**
308 **5D**).

309 The B-type motor neurons are required for forward locomotion (Chalfie et al., 1985; Wen et al.,
310 2012), and are rhythmically active during forward locomotion (Haspel et al., 2010; Kawano et
311 al., 2011; Wen et al., 2012). We sought to determine whether any individual or small group of
312 these neurons is essential for 2FU. We ablated groups of 2-6 B-type motor neurons at a time
313 using our pulsed infrared laser system. 2FU occurred at least rarely in each condition (**Figure**
314 **4C, F; Figure 4 Figure Supplements 3, 4**), suggesting that no specific B cell body is essential
315 for 2FU. In nearly all cases, ablation of a DB motor neuron resulted in the disappearance of its
316 commissural process, but we could not determine whether ablated VB neuronal processes were
317 similarly removed. Therefore, we cannot completely exclude the possibility that a specific
318 neuronal process can generate rhythms for 2FU in the absence of its associated cell body.

319 Taken together, these results suggest that in the presence of premotor interneurons, the B
320 and/or AS class motor neurons contribute to neck-paralysis induced 2FU, but no single member
321 is essential for generating high frequency tail rhythms during 2FU. The A, VC and D motor
322 neurons are not required for 2FU. Our results are consistent with a model in which posterior
323 rhythm generation can arise from multiple subsets of B or AS motor neurons.

324

325 **B-type motor neurons, as a class, are essential for 2FU**

326 We next asked whether the B motor neurons as a class are required for 2FU. We first
327 considered *vab-7* mutants, in which the DB motor neurons have aberrantly reversed processes.
328 These worms have disrupted wave propagation in the tail, which coils towards the ventral side
329 (Wen et al., 2012). We found that *vab-7* mutants had mildly or strongly paralyzed tails and were
330 incapable of 2FU when neck muscles were inhibited, suggesting that *vab-7* is essential for 2FU
331 **(Figure 4 Figure Supplement 1D, E)**.

332 The inability of *vab-7* worms to generate the high frequency tail oscillation is consistent with the
333 notion that broad disruption of the B motor neurons prevents 2FU. However, the behavioral
334 deficit could also result from other effects of the mutation.

335 To ascertain whether the B motor neurons are required for 2FU, we performed broad ablations
336 of the B motor neurons. We studied worms expressing P*unc-17::PH::miniSOG* (Xu and
337 Chisholm, 2016). In our integrated lines, we found that illumination of P*unc-17::PH::miniSOG*
338 worms preferentially eliminated the DA and DB over the VA and VB motor neurons (see
339 Methods). Worms in which most DB motor neurons were eliminated were dramatically less likely
340 to show 2FU than mock controls, but were not incapable of doing so (**Figure 5, Video 4**; N=9
341 out of 104 trials from 25 worms by blinded, randomized scoring). We performed the converse
342 experiment – elimination of most VB motor neurons using our infrared laser system— and found
343 the incidence of 2FU was again sharply reduced but not eliminated (**Figure 5, Video 4, Figure**
344 **5 Figure Supplement 1**). When we combined miniSOG and laser ablation to remove all DB and
345 most VB motor neurons, animals were incapable of 2FU (**Figure 5**; 0 out of 102 trials from 27
346 worms by blinded, randomized scoring).

347 Taken together, these results suggest that the B motor neurons as a class are essential for
348 independent tail undulation during forward movement. Our results are consistent with the
349 hypothesis that the B motor neurons have a role in generating the high frequency locomotory
350 rhythm observed in 2FU.

351

352 **Multiple lesion-separated VNC segments are capable of independent rhythm generation**

353 The observation that 2FU could persist despite disruptions to many components of the mid-body
354 motor circuitry could also be explained by the hypothesis that additional rhythm generators
355 located in the head are responsible for the observed high frequency tail undulations. Although

356 the premotor INs account for the majority of synaptic inputs to the VNC motor neurons, there
357 are additional connections between head neurons and the anterior VNC motor neurons that
358 bypass the premotor INs (White et al., 1986).

359 To ascertain whether the mid-body motor circuit is capable of independent rhythm generation,
360 we developed a method for eliminating synaptic connections between the mid-body motor
361 neurons and the head circuits. We used our infrared laser system to sever both the VNC and
362 the dorsal nerve cord (DNC) just posterior to the pharynx. In many cases, this procedure also
363 severed other fasciculated process bundles that run parallel to the VNC and DNC (**Figure 6A**).

364 Several hours after disruption of the nerve cords, most animals were inactive (data not shown),
365 but active forward locomotion was induced by application of a mechanical stimulus. Most of
366 these worms could generate robust oscillations posterior to the cut location (**Figure 6A, E,**
367 **Video 5**). Moreover, the tail often undulated at a higher frequency than the mid-body (**Figure**
368 **6E**). In these worms, oscillations in the head were highly disrupted. In some cases, low
369 amplitude waves propagating in the posterior-to-anterior direction occurred simultaneously with
370 robust mid-body and tail waves propagating in the anterior-to-posterior direction (**Figure 6A,**
371 **Video 5**), suggesting a deficit in coordination between circuits on either side of the lesion. These
372 results suggest that synaptic connections from the head circuits to the motor neurons may not
373 be essential for wave generation posterior to the head.

374 We considered the possibility that under these conditions, mid-body undulations were being
375 caused by small movements in the head rather than generated by a second oscillator. To
376 minimize the small movements of the head, we introduced an additional manipulation to reduce
377 head movement. Using our infrared laser, we applied thermal damage to the worm's nerve ring
378 (located in the head) in addition to cutting both nerve cords. Animals treated with these three
379 lesions are henceforth referred to as "VNC-lesioned" worms. These worms exhibited very little

380 movement in the head. However, they continued to generate robust oscillations in the mid-body
381 and even higher frequency oscillations in the tail (**Figure 6B, E, Video 5**). The pattern of
382 locomotion in VNC lesioned animals strongly resembled the 2FU induced by optogenetic
383 perturbation, with the important difference that in our lesioned preparation, both frequencies
384 were likely generated *outside* the head.

385 The emergence of multiple frequencies of undulation outside the head suggests that the VNC
386 motor circuit itself may contain multiple units capable of independent oscillation. These units
387 may exist in addition to any oscillating unit(s) in the head. To test this possibility directly, we cut
388 the VNC and DNC in two locations: in the neck (anterior to VB3) and in the tail (posterior to
389 VB8). We again thermally lesioned the head neurons to suppress head movement. Under these
390 conditions, the VNC motor neurons between VB3 and VB8 are isolated from circuitry in both the
391 head and tail, and the VNC motor neurons posterior to VB8 are isolated from both the head
392 circuits and the anterior VNC motor neurons. As before, these animals could generate robust
393 body oscillations posterior to the first cut and higher frequency oscillations posterior to the
394 second cut (**Figure 6C, E, Video 5**), suggesting that rhythms can arise independently from each
395 of these portions of the VNC motor neurons. It should be noted that in all of our VNC lesion
396 studies, the processes of premotor interneurons AVA, AVB, and PVC likely remained present in
397 the VNC.

398

399 **B class motor neurons are necessary for rhythmic wave generation in VNC-lesioned**
400 **worms**

401 We next asked which motor neuron groups contributed to rhythm generation in worms in which
402 the VNC and DNC were severed. The A motor neurons are not necessary for 2FU induced by
403 neck paralysis (Figure 4 - Figure Supplement 1C). We hypothesized that they are similarly not

404 required for body oscillation in VNC-isolated worms. We severed the VNC and DNC in either
405 one or two locations after ablating the A motor neurons with P*unc-4::miniSOG*. Animals in which
406 the VNC and DNC had been severed near the head were capable of robust wave generation
407 and propagation posterior to the head (Figure 6 - Figure Supplement 1B). Animals in which the
408 VNC and DNC were severed in two locations were capable of rhythmic activity in the mid-body
409 or tail, although we did not observe any cases of simultaneous oscillation in each segment
410 (N=20 worms, Figure 6 - Figure Supplement 1C). These results support the idea that the A
411 motor neurons are not required for generation of rhythmic forward waves in surgically isolated
412 segments of the VNC motor circuit.

413 The B motor neurons were required for neck-paralysis-induced 2FU in intact animals (Figure 5).
414 We hypothesized that they are also required for forward undulatory rhythms in VNC-lesioned
415 worms. To test this idea, we used VNC-lesioned worms in which the DA and DB motor neurons
416 were ablated by miniSOG and the VB motor neurons were ablated by an infrared laser as
417 before. Three to five hours after nerve cord surgery, worms in either B-ablation condition, like
418 mock controls, were highly inactive. Application of a mechanical stimulus caused tight coiling,
419 especially but not exclusively in the DB-only ablation condition (**Figure 6 Figure Supplement**
420 **2C, Video 6)**. Despite this coiling, we observed at least one case of a VNC-lesioned, DB-
421 ablated worm appearing to move the very tip of its tail, possibly in a rhythmic fashion,
422 suggesting that DB neurons may not be required for rudimentary oscillation in at least the most
423 posterior portion of the tail. However, in VNC-isolated worms for which most DB and VB
424 neurons were ablated, we never observed rhythmic movements (**Figure 6 Figure Supplement**
425 **2D-F**; N=19 mechanical stimulus trials from 9 worms). These results suggest that, as was the
426 case for optogenetic 2FU, the B motor neurons are required for rhythm generation in VNC-
427 lesioned worms.

428 The observation that anterior VNC/DNC cuts disrupt normal head undulation (**Figure 6A**)
429 suggests that rhythm generation by the head circuit may require inputs from the VNC. To
430 address this possibility, we studied additional worms in which the VNC/DNC were cut in 2
431 locations slightly more posterior to the head to reduce the likelihood of damage to the head
432 motor neurons, but which were not subject to thermal damage to the head. As in our earlier
433 experiment (Figure 6A), head movement was severely disrupted (not shown). However, we
434 occasionally observed very slow head undulation in these animals, indicating that head
435 undulation is still possible under these conditions (**Figure 6D**, **Video 5**).

436 One explanation for the low frequency of head undulations is that damage to the SMB or SMD
437 neurons in the parallel tracts (**Figure 6A**) hampered head movement. Another possibility is that
438 input from the posterior motor circuit is essential for the normal frequency of head undulation.
439 The first hypothesis may be supported by our earlier observation that strong decoupling of head
440 and tail oscillations by muscle ablation (i.e. *without* lesioning the nerve cord or parallel tracts)
441 resulted in similarly slow head oscillations (**Figure 3D**), while weak decoupling resulted in
442 moderately slower head oscillations (**Figure 3A**). The possibility of posterior-to-anterior
443 communication is discussed in detail in later sections.

444 These results suggest that the *C. elegans* forward locomotor circuitry possesses at least three
445 units capable of independent oscillation, with two units located outside the head. Although we
446 did not observe simultaneous 3-frequency forward undulation in any animal tested, we have
447 shown that oscillations are possible in each segment when isolated from the others.

448

449 **Undulations can arise in arbitrary portions of the VNC motor circuit**

450 We next sought to identify the smallest portion of the VNC motor circuit that is capable of
451 generating rhythmic behaviors, and whether any differences exist between the rhythmic

452 properties of segments of various sizes. To address these questions, we again damaged the
453 head (as in Figure 6B), then systematically varied the location of VNC/DNC lesions relative to
454 the B motor neurons.

455 When we severed the VNC and DNC at any one of a number of different locations (anterior to
456 VB3, VB5, VB6, VB7, VB9, VB10, and VB11), we found that undulations posterior to the
457 damage arose near each cut location (**Figure 7B-E**). Bending amplitude similarly recovered just
458 posterior to each cut location, rather than at a fixed body coordinate (**Figure 7F**). Oscillations in
459 the tail usually had a higher frequency when the nerve cords were severed in the tail than when
460 they were severed near the head (**Figure 7G**). We did not observe any bouts of locomotion with
461 anterior-to-posterior waves posterior to the lesions when we severed the nerve cords anterior to
462 VB11 (not shown), and bouts detected after lesioning at VB10 had waves of very low amplitude
463 (**Figure 7F**), without clear rhythmicity (not shown). The smallest VNC segment that produced
464 clear and robust rhythmic waves was the region between VB9 and the tail. These results
465 suggest that the most compact rhythm-generating unit of the forward motor circuit is at least as
466 small as the region containing VB9, VB10, VB11, DB6, and DB7.

467

468 **Rhythmic motor entrainment is possible in both the anteriorward and posteriorward**
469 **directions**

470 Although we have shown that the *C. elegans* forward motor circuitry contains multiple rhythm
471 generating units, it remains unclear exactly how these oscillators are coupled together, or even
472 if they are all active during normal locomotion. Previous work demonstrated proprioceptive
473 coupling in the posterior direction (Wen et al., 2012), and we showed that a disruption to
474 proprioceptive coupling, via optogenetic inhibition of neck muscles, could decouple body
475 undulations from head movements (**Figures 3A, 4**). One surprising feature of our results was

476 that paralyzing the neck muscles appeared to decrease the head frequency. We found that
477 during 2FU, head frequency decreases relative to the unperturbed swimming frequency (**Figure**
478 **8A**). Slowing was often even more dramatic when decoupling was stronger (**Figures 3D, 6D**).
479 These observations suggest that anteriorward coupling, in addition to posteriorward coupling,
480 may be present in the forward locomotor circuitry.

481 To test for anteriorward coupling between motor circuit elements, we asked whether an
482 oscillating optogenetic perturbation in the mid-body can entrain the head to a new frequency.
483 We used our optogenetic targeting system to rhythmically inhibit the mid-body BWMs (**Figure**
484 **8B**). Worms subject to this procedure exhibit a head bending frequency approximately one half
485 that of the imposed frequency. The factor of one half is likely due to the presence of two phases
486 during the rhythmic locomotory cycle of any single part of the body during which the curvature is
487 close to zero (i.e. muscles are relaxed). In some cases, small head bends corresponding to
488 individual mid-body pulses were evident as well (**Figure 8C(i), Video 7**).

489 We found the head frequency could be entrained to a range of imposed mid-body frequencies.
490 Subjecting body coordinates 33-66 to pulsed illumination at frequencies from approximately 1 to
491 2 Hz caused an increase in the power spectrum of the worm's oscillations at frequencies
492 corresponding to half of the imposed frequency, and a decrease at other frequencies. Pulsing at
493 frequencies below 1 Hz generally led to head oscillations near the imposed frequency (**Figure**
494 **8C(ii)**). These results show that a mid-body rhythmic signal can entrain head bending, and
495 point to the presence of an anteriorward coupling mechanism within the motor circuit.

496 We asked whether the anteriorward coupling occurs via the VNC cholinergic neurons, which are
497 electrically coupled to each other, the muscle-to-muscle gap junctions, or through another
498 mechanism. We applied a rhythmic optogenetic inhibition pattern to the midbody cholinergic
499 neurons in P*unc-17::NpHR* worms. Once again, worms subject to this procedure quickly adjust

500 their head bending frequency to match one-half of the imposed frequency (**Figure 8D(i), Video**
501 **7**). Moreover, rhythmic illumination of the tail cholinergic neurons at 2 Hz similarly increased the
502 magnitude of head bending at 1 Hz (**Figure 8D(ii)**). Selective rhythmic hyperpolarization of the
503 mid-body B motor neurons also sufficed to increase the magnitude of head bending at one-half
504 of the stimulus frequency (**Figure 8 - Figure Supplement 1A**), as did rhythmic
505 hyperpolarization of the BWMs when muscle-to-muscle gap junctions were disrupted in only in
506 the BWM by a mutation in the innexin *unc-9* that was rescued in neurons but not muscles (Wen
507 et al., 2012) (**Figure 8 - Figure Supplement 1B**). These observations suggest that the posterior
508 to anterior coupling is mediated neuronally, possibly by the VNC motor neurons.

509

510

511 **DISCUSSION**

512 In zebrafish and lampreys, rhythmogenic capability for swimming undulations is distributed
513 along the rostro-caudal axis of the spinal cord (Kiehn, 2006; Mullins et al., 2011). When isolated
514 from the rest of the cord, groups of lamprey spinal segments do not exhibit identical preferred
515 frequencies (Cohen, 1987). In the swimming intact animal, oscillations in all segments are
516 phase and frequency-locked by intersegmental coupling that spans broad swaths of the spine
517 (Mullins et al., 2011).

518 The motor system of the leech, an invertebrate, also shows a distributed rhythm generating
519 architecture. Individual ganglia of the leech VNC can generate crude bursting patterns that
520 resemble their firing patterns during swimming. The most robustly oscillating ganglia are
521 towards the middle of the leech's body, and isolated midbody ganglia also have a higher
522 frequency than isolated ganglia near either the head or tail. In the intact animal, extensive,
523 bidirectional intersegmental coupling drives the system to adopt a single locomotor frequency
524 (Pearce and Friesen, 1985; Kristan et al., 2005).

525 Our results reveal a picture of forward locomotor control in *C. elegans* similar to that found in
526 lamprey and leech. We found that rhythmogenic capability in the worm is distributed along the
527 VNC motor circuit. As in other swimming models, the rhythm-generating capability of posterior
528 circuits is only detectable when coupling is disrupted. The rhythm-generating capability of
529 posterior circuits was demonstrated in several ways: optogenetic inhibition of anterior neurons,
530 optogenetic inhibition of anterior muscles, an inhomogeneous mechanical environment, or a
531 lesion to the nerve cords. The incomplete nature of our optogenetic decoupling method yielded
532 evidence that an anterior rhythm can entrain the higher-frequency posterior rhythms. For
533 example, we found that during 2FU, some but not all waves in the tail were continuous with

534 waves in the head (**Figure 3B, C**). Even in these cases, the difference in locomotory frequency
535 between the two body regions is inconsistent with single oscillator models.

536 We found that neither the head nor tail frequency during 2FU matched the natural (unperturbed)
537 frequency of locomotion. Instead, the normal locomotory frequency in the environment of the
538 assay was generally intermediate between the head and tail frequencies exhibited during 2FU.
539 This finding shows another key similarity with models of swimming in other vertebrates and
540 invertebrates: during locomotion, multiple rhythm generating units, each with different rhythmic
541 properties, are combined by strong inter-unit coupling to form one functional unit (Friesen and
542 Hocker, 2001; Kristan et al., 2005; Kiehn, 2006; Mullins et al., 2011). Such a whole-body
543 oscillating unit will generally have rhythmic properties different from that of any subunit in
544 isolation. Indeed, modeling studies of the leech swim CPG have suggested that the overall
545 fictive locomotor frequency of a 17-ganglion portion of the VNC lies within the range of
546 frequencies of the individual ganglia (Zheng et al., 2007). The gradient in intrinsic frequencies
547 appears to set the wavelength during fictive swimming. The variation in rhythmic properties
548 between different parts of the body may play a similar role in *C. elegans.*

549 During forward locomotion, the *C. elegans* motor circuit is coupled by posteriorward
550 proprioception (Wen et al., 2012), and additional anteriorward and posteriorward coupling
551 mechanisms (**Figure 8**). This bidirectional coupling appears to allow the entire circuit to operate
552 as one unit. This picture is similar to descriptions of leech and lamprey motor circuits. In the
553 leech, oscillatory interneurons that comprise the swim CPG send axons along the anterior-
554 posterior axis of the animal, and mediate bidirectional coupling between midbody ganglia
555 (Friesen and Hocker, 2001; Kristan et al., 2005). The coupling between ganglia appears to
556 result from a mixture of proprioceptive feedback and central control (Yu et al., 1999; Kristan et
557 al., 2005). Injection of sinusoidally varying current into the leech stretch receptor cells was
558 sufficient to entrain swimming activity (Yu and Friesen, 2004) at the injection frequency.

559 Imposed rhythmic movements are also capable of entraining fictive swimming in isolated
560 preparations of the lamprey spinal cord (Grillner et al., 1981; McClellan and Sigvardt, 1988) and
561 several other vertebrate and invertebrate systems (Wendler, 1974; Andersson et al., 1981;
562 Robertson and Pearson, 1983).

563 Our results include several lines of evidence implicating the cholinergic B and AS motor neurons
564 as a likely source of posterior rhythmogenesis during *C. elegans* forward locomotion. First,
565 disruption or removal of most or all B motor neurons virtually abolished independent tail
566 undulations induced either optogenetically or by severing the nerve cords, but elimination of
567 other motor neurons and premotor interneurons did not eliminate the ability of the posterior to
568 oscillate independently (**Figures 4, 5, and 6**). Second, stimulation of select B and AS neurons
569 after paralyzing most of the body led to local, high frequency oscillations in the tail that
570 mimicked 2FU (**Figure 3 Figure Supplement 1**). Third, imposing a rhythmic signal on mid-body
571 B motor neurons sufficed to entrain whole-body locomotor frequency, as did imposing rhythms
572 on the broader class of cholinergic neurons and the body wall muscles; changes in body
573 posture are sensed by the B motor neurons (Wen et al., 2012), providing a likely explanation for
574 how this manipulation was able to entrain locomotion. The latter argument is somewhat
575 comparable to one of the key criteria used to classify leech interneurons as part of the swim
576 CPG; that injection of a pulse of current resets the phase of the locomotor rhythm (Mullins et al.,
577 2011). In our experiments, the swimming frequency, and thus phase, was reset almost
578 immediately after the first inhibitory stimulus, suggesting that the B motor neurons share the
579 phase shifting property with oscillatory interneurons in the leech. Lastly, the B motor neurons
580 are rhythmically active in phase with locomotion (Kawano et al., 2011; Wen et al., 2012),
581 satisfying another key criterion set for candidate oscillator neurons in the leech (Mullins et al.,
582 2011).

583 Descriptions of swimming CPGs in vertebrates have tended to exclude motor neurons as
584 members of the CPG, with most oscillatory function attributed to interneurons (Kiehn, 2016).
585 Leech excitatory motor neurons have not been shown to be members of the swim CPG, as
586 injection of a pulse of current fails to reset the cycle phase (Kristan et al., 2005). However, leech
587 inhibitory motor neurons are ascribed a role in swimming rhythm generation using the phase-
588 resetting criterion (Mullins et al., 2011), motor neurons comprise the crab stomatogastric CPG
589 (Marder and Bucher, 2007), and recent work has shown that motor neurons are key
590 components of several locomotory pattern generators. In leech crawling, which consists of cyclic
591 elongation and contraction phases, current pulses to the CV elongation motor neurons do
592 indeed reset the phase of fictive crawling. However, the CV neurons were not concluded to be
593 necessary components of the CPG because tonic hyperpolarization failed to abolish the
594 crawling rhythm. Anatomical removal, arguably the more relevant test of necessity, was not
595 reported (Rotstein et al., 2017). In zebrafish, motor neurons for swimming are bidirectionally
596 coupled to locomotion-driving interneurons by gap junctions, and influence their recruitment,
597 synaptic transmission, and firing frequency during locomotion (Song et al., 2016). Hence, there
598 is a growing recognition that motor neurons are not limited to conveying oscillatory signals from
599 interneurons, but may themselves participate in rhythm generation.

600 One difference between our results and previous findings in leeches is in the effect of severing
601 the VNC. When we severed the VNC and DNC of *C. elegans*, we found that independent,
602 generally higher frequency undulations occurred posterior to the severed region (**Figures 6 and**
603 **7**). Disruption of the leech VNC, by contrast, was not sufficient to prevent wave propagation
604 from head to tail (Yu et al., 1999), suggesting that proprioceptive information suffices to
605 propagate the wave. However, severing the VNC intersegmental coordinating neurons in *in vitro*
606 preparations induced uncoordinated fictive swim oscillations at different frequencies occurring
607 on either side of the cut (Weeks, 1981). This difference in results may arise due to differences

608 between our thermal ablation method in *C. elegans* and physical severing of the leech VNC, or
609 the relative span of proprioceptive signals in each system.

610 Our laser lesioning of the VNC likely did not remove processes of premotor interneurons, nor
611 did it prevent nonsynaptic neurotransmission, for example through neuropeptides, from
612 potentially regulating rhythm generation across the lesion. These possibilities may account for
613 the apparent difference in posterior rhythmogenic capability between worms in which AVB had
614 been ablated versus severed. When the ventral nerve cord was isolated from the head ganglia,
615 including the soma of AVB, rhythmic tail undulation was reliably evoked by a mechanical
616 stimulus (**Figures 6 and 7**). However, independent tail undulations were observed only rarely
617 after ablating AVB, even when the mechanical stimulus was applied (**Figure 4 Figure**
618 **Supplement 1**). The AVB process that likely remain in the severed VNC segments may
619 continue to provide excitation to the B motor neurons to promote rhythm generation. The other
620 apparent discrepancy, between disrupting AVB-B gap junctions by *unc-7* or *unc-9* genetic
621 mutations and ablating AVB, may be a consequence of other effects of the mutation, including
622 changes in other connections between the premotor interneurons and the B motor neurons
623 (Starich et al., 2009), that may compensate for the loss of AVB:B gap junctions to activate the
624 forward circuit. In any case, the observation that tail undulation was observed at least rarely in
625 all three conditions is inconsistent with the notion that AVB is required for rhythm generation in
626 the VNC motor circuit.

627 Taken together, our results point to a new working model of *C. elegans* forward locomotion
628 (**Figure 9)**. Three oscillator units are depicted: an unknown head CPG, the VNC motor neurons
629 between VB3 and AS7, and the VNC motor neurons between VB9 and AS11. The two VNC
630 units are justified by our data from worms in which the VNC and DNC were cut in multiple
631 locations (**Figure 6C**). We include AS in the model because it is the only class of VNC motor
632 neurons that we have not directly investigated in our 2FU assay, and could be important for

633 rhythm generation in the tail. These are not the only circuit units capable of generating
634 oscillations; when we severed the VNC and DNC at arbitrary locations we found that oscillations
635 resume closely posterior to each cut over a wide range of circuit sizes (**Figure 7**). Moreover, we
636 cannot rule out the possibility that even smaller circuit units, perhaps even individual motor
637 neurons, can generate rhythmic outputs.

638 Dissecting the relative contributions of cellular pacemakers, network oscillators, and reflex loops
639 to rhythmic motor generation and coordination has been a longstanding challenge in vertebrates
640 and invertebrates (Kristan et al., 2005; Kiehn, 2006). Our finding that the architecture for rhythm
641 generation in *C. elegans* locomotion shares key properties with other vertebrate and
642 invertebrate models sets the stage for molecular, cellular, and network-level investigations of
643 motor coordination in a uniquely tractable model organism.

644

**Figure 1. Overview of curvature analysis and models of rhythm generation**

(A) Dark field image of worm shown with curvature segmentation. Dorsal bending is shown in blue and ventral bending in red. The dorso-ventral orientation is arbitrary unless otherwise specified. The worm's centerline is used to define a coordinate system in which the head and tail are located at body coordinates 0 and 100, respectively. Scale bar: 200 μm.

(B) Curvature map from a normally swimming worm. The curvature at time t = 0 s corresponds to the image shown in (A).

(C) In a single-oscillator model of locomotion, an unknown oscillator causes rhythmic head bending, and a reflex-like coupling mechanism mediates propagation of these bends along the rest of the body.

(D) A multi-oscillator model (Gjorgjieva et al., 2014) posits the existence of additional circuit units outside the head capable of generating oscillations.

(E) Conceptual curvature map showing predicted worm behavior after paralyzing a small region of the body (dotted white box). The single-oscillator model predicts that all regions posterior to the paralyzed region will also become paralyzed.

(F) Conceptual curvature map predicting the outcome of the same manipulation applied to a multi-oscillator model. If additional oscillators exist posterior the paralyzed region, additional tail oscillations may arise, potentially with different amplitude, frequency, and/or phase.

**Figure 2. Anterior undulation is not required for posterior undulation**

(A) Inhibition of anterior BWMs (via P*myo-3::NpHR*) increases tail frequency. Body coordinates 0-45 were illuminated with green light (532 nm wavelength) to trigger relaxation of the anterior muscles. The spatiotemporal extent of green laser illumination is indicated by the white dotted box.

670 (B) Inhibition of anterior cholinergic neurons (via P*unc-17::NpHR*; P*unc-17::ChR2*) does not
671 prevent tail undulation. Body coordinates 0-33 were illuminated with green light to
672 optogenetically inhibit anterior motor activity.
673 (C) Tail undulations persist despite paralysis of the anterior BWMs due to miniSOG-mediated
674 lesion of muscle cells. Animals were subjected to mechanical stimulation to induce locomotion
675 (see Methods). A total of 9 animals were illuminated with blue light (472 nm wavelength) in
676 approximately their anterior halves. Of these, 5 displayed partial-body forward swimming as
677 depicted here, 3 were immobile, and one was not sufficiently paralyzed in the head. Six control
678 worms, which were mounted identically but not illuminated, all displayed waves propagating
679 normally from head to tail (not shown).
680 (D) Inhibition of some anterior muscles (body coordinate 0-33, N=10 worms) significantly
681 increases tail frequency. Inhibition of most anterior muscles (0-45, N=10 worms), or inhibition of
682 anterior cholinergic neurons (N= 14 worms) produces mixed results; some animals generate
683 high frequency tail oscillations while others slow down. Each colored circle represents one trial;
684 worms may have multiple trials. Tail frequency is measured at body coordinate 85. Error boxes
685 represent the mean and SEM.
686 (E) Amplitude of undulation in the head and tail before and during muscle or neuron inhibition.
687 Head frequency is measured at body coordinate 15. Note sharp decreases in head amplitude
688 during all three manipulations. Amplitude here and henceforth is measured as the root mean
689 square of the time derivative of the curvature times worm length $\mathrm{rms}\left(L \cdot \frac{d\kappa}{dt}\right)$ and has units of $s^{-1}$.
690 (*) $p<0.05$; (**) $p<0.01$; (***) $p<0.001$; paired t-test.
691
692
693 **Figure 3. Disruption of motor coupling in the neck de-synchronizes head and tail**
694 **oscillations**

695 (A) Inhibition of neck BWMs (via P*myo-3::NpHR*) increases tail frequency and decreases head
696 frequency. We refer to this effect as two frequency undulation (2FU). Body coordinates 25-45
697 were illuminated with green light to induce relaxation of neck muscles. The spatiotemporal
698 extent of green laser illumination is indicated by the white dotted box.
699 (B,C) Inhibition of neck cholinergic neurons (P*unc-17::NpHR*) or neck B-type motor neurons
700 (P*acr-5::Arch*) also induces 2FU behavior.
701 (D) Two frequency undulation after miniSOG-induced paralysis of the mid-body BWMs. Animal
702 was subjected to mechanical stimulation to induce locomotion, but also displayed this behavior
703 prior to stimulation. A total of 10 individuals were illuminated with blue light on approximately
704 one-fifth of their body length, centered near the vulva. Of these, 7 displayed 2FU as depicted
705 here, one was immobile, and two were not sufficiently paralyzed in the mid-body to disrupt
706 bending waves. Color map data is scaled down by 50% because bends in this animal had
707 higher amplitudes than those shown in A-C.
708 (E) Several optogenetic manipulations produced decoupled head and tail oscillation. 2FU is
709 assayed by dividing tail frequency by head frequency in each worm. Before illumination, the
710 head (body coordinate 15) and tail (body coordinate 85) usually oscillate at the same frequency.
711 During illumination, tail frequency often exceeds head frequency. Each colored circle pair
712 represents one trial; worms may have multiple trials. N= 11, 10, 12, and 10 worms per condition,
713 respectively. Error boxes represent the mean and SEM.
714 (F) Amplitude of undulation in the neck and tail before and during neck muscle or neuron
715 inhibition. Neck amplitude is measured at body coordinate 35. (*) $p<0.05$; (**) $p<0.01$; (***)
716 $p<0.001$; paired t-test.
717
718 **Figure 4. VNC premotor interneurons, D-type motor neuron signaling, and individual B-**
719 **type motor neurons are not required for 2FU**

720 (A) 2FU occurs despite ablation of premotor interneurons (P*glr-1::ICE*; P*myo-3::NpHR*). The
721 spatiotemporal extent of green laser illumination is indicated by the white dotted box.
722 (B) 2FU occurs despite disruption of AVB:B gap junctions and BWM:BWM gap junctions (*unc-9*;
723 P*myo-3::NpHR*)
724 (C) 2FU occurs despite ablation of a small subset of the B-type motor neurons (P*myo-3::NpHR*;
725 P*acr-2::wCherry)*. VB8, VB9, and DB6 were ablated using our pulsed infrared laser system.
726 (D) 2FU occurs despite elimination of GABAergic signaling (*unc-49;* P*myo-3::NpHR*)
727 (E) When subjected to neck paralysis (P*myo-3::NpHR*; P*acr-2::wCherry*), 2FU occurs reliably in
728 P*glr-1::ICE* animals and occasionally in *unc-9* and *unc-49* animals. Each colored circle pair
729 represents one trial; worms may have multiple trials. N = 12, 8, and 10 worms per condition,
730 respectively. Head frequencies are measured at body coordinate 15. Mid-body are frequencies
731 are measured at body coordinate 60. Error boxes represent the mean and SEM.
732 (F) When subjected to neck paralysis (P*myo-3::NpHR*), 2FU occurs at least occasionally despite
733 ablation of subsets of the B-type motor neurons by our pulsed infrared laser system. For each
734 condition, data is only considered from worms that have all specified neurons missing; some
735 worms in each group may have additional B-type or other neurons missing. N= 40, 30, 32, 27,
736 18, 18, and 16 trials from 10, 10, 10, 8, 7, 7, and 7 worms per condition, respectively. (*) $p<0.05$;
737 (**) $p<0.01$; (***) $p<0.001$; paired t-test.
738
739 **Figure 5. B motor neurons are required for 2FU**
740 (A) Top panels: assessment of ablations using a P*acr-2::mCherry* label. After removal of dorsal
741 B motor neurons (P*unc-17β::PH::miniSOG*), pairs of motor neurons – each corresponding to
742 one VA and one VB type neuron – are visible along the VNC (blue arrows). Neither the DNC
743 (red arrows) nor the DB or DA commissures (red arrowheads in mock) are visible. Scale bars:
744 100 μm.

745 Bottom panels: Corresponding examples of worm locomotion after removal of DB (via miniSOG)
746 and VB (via IR laser) motor neurons. Removal of DB always resulted in tail paralysis in a coiled
747 position, but a minority of worms were able to generate a rhythmic midbody wave. Additional
748 removal of VB motor neurons by laser ablation completely prevented 2FU and resulted in
749 severe tail paralysis. (B,C) 2FU, as assayed by frequency measurements (B) or blinded,
750 randomized scoring (C), is sharply reduced or eliminated by removal of DB, VB, or both. Head
751 and mid-body frequencies were measured at body coordinates 15 and 60, respectively. Error
752 boxes in (B) are the mean and 95% confidence interval of the mean. Error bars in (C) are
753 standard error of the sample proportion. Numbers above each bar in (C) indicate the number of
754 trials scored 2FU over the total number of trials for the condition; each individual worm
755 contributed between 1 and 5 trials (3.6 on average). (***) $p<0.001$; paired t-test.
756
757 **Figure 6. Undulations generated in the tail after severing the dorsal and ventral nerve**
758 **cords**
759 (A) The VNC (blue arrow) and DNC (red arrow) were severed in a P*unc-17::GFP* worm using a
760 pulsed infrared laser. Several other dorso-ventral processes also appear cut. Nonetheless,
761 robust bending waves are generated in the mid-body (lower pane). All scale bars: 50 μm.
762 (B) The VNC and DNC are severed, and arbitrary damage has been applied to the nerve ring to
763 suppress head movements. Robust bending waves are generated in both the neck and tail
764 (lower pane).
765 (C) The VNC and DNC are severed posterior to the head and vulva (P*acr-2::wCherry*), and the
766 nerve ring is lesioned to suppress head movements. Robust bending waves are generated in
767 both the neck and tail (lower pane).
768 (D) The VNC and DNC are severed posterior to the head and vulva, but the nerve ring was not
769 targeted. Low frequency head undulation and high frequency tail undulation were observed
770 separately in this animal.

(E) Frequency of undulation in the mid-body and tail for all ablation conditions and mock controls. Each colored circle pair represents one bout of forward locomotion lasting at least 2 s. For each condition, data is only considered for worms in which the VNC and DNC are clearly severed in the indicated locations. Mid-body and tail frequencies were measured at body coordinates 45 and 85, respectively. Error boxes represent the mean and SEM. N = 3, 7, 3, 4, 5, and 7 worms per condition, respectively. (*) $p<0.05$; (**) $p<0.01$; (***) $p<0.001$; paired t-test.

**Figure 7: Undulations are generated after VNC/DNC lesioning in arbitrary locations**

(A) Schematic indicating all regions at which we severed the VNC and DNC in relation to the B motor neurons. Each animal's nerve cords were severed at only one of these locations. The nerve ring of each worm was also damaged to restrict head movements as in Figure 5B.
(B-E) Representative curvature maps for worms subject to four of the tested conditions. Note that anterior-to-posterior waves begin progressively more posterior for each cut location. In some cases, the head and tail exhibited waves propagating in opposite directions (D).

(F) Amplitude of bending as a function of body coordinate after severing the VNC and DNC anterior to the indicated motor neuron. Only the portion of the curve posterior to the amplitude minima (the cut location) is shown. No bouts of locomotion with anterior-to-posterior waves were discernible posterior to the cut at VB11 either subjectively or by our analysis software. For cut locations at VB3, VB5, VB6, VB7, VB9, VB10, and VB11 we studied N = 15, 9, 6, 10, 14, 9, and 6 worms and observed 25, 16, 7, 12, 30, 19, and 14 bouts of forward locomotion (lasting at least 3 s), respectively. Shaded outline represents ±SEM.

(G) Frequency of undulation at body coordinate 75 for four cut conditions. Boxes represent mean and SEM. Each colored circle indicates the frequency during one bout of forward locomotion. *p<0.05, one-way ANOVA with Bonferroni post-hoc comparisons.

**Figure 8. Head undulation frequency can be entrained by mid-body optogenetic manipulation**

(A) Neck muscle hyperpolarization (Figure 3A) causes a significant decrease in head bending frequency. This decrease is not predicted by either model discussed in Figure 1.

(B) A multi-oscillator model of forward locomotion allowing for motor coupling in both the anterior and posterior directions. To test this model, we sought to impose a new frequency on the mid-body of a freely moving worm, and test whether head bending also adopts the new frequency.

(C) Head bending frequency can be entrained by rhythmically inhibiting the mid-body BWMs.

(i) A curvature map showing a representative trial. Green light was pulsed on coordinates 33-66 at a frequency of 2 Hz onto a P*myo-3::NpHR* worm. Note that the head frequency slows to half of the imposed frequency, although some instances of a 1:1 correlation between laser pulse and a head bend are also evident (e.g. around t = 13 s).

(ii) Mean head frequency power spectra of P*myo-3::NpHR* worms before manipulation (left bar, worms from all conditions are pooled) and while subject rhythmic mid-body paralysis. Frequencies tested were 0 (with laser on), 0.5, 0.85, 1.1, 1.25, 1.4, 1.55, 1.7, 1.9, and 2.0 Hz. Frequency data is interpolated between these points. N≥11 trials per condition, with each worm supplying at most two trials. For high frequency inhibition (f>1.1 Hz) the head is entrained to half of the inhibition frequency (bright peaks lie along y=x/2). For lower frequencies of inhibition (f~0.85 Hz) the head is entrained to the inhibition frequency (bright peaks lie along y=x).

(D) Head bending frequency can be entrained by rhythmically inhibiting the head, mid-body, or tail cholinergic neurons.

819 (i) A curvature map showing a representative trial. Green light was pulsed on coordinates 33-66
820 at a frequency of 2 Hz onto a P*unc-17::NpHR* worm.
821 (ii) Mean head frequency spectra before manipulation (black, all conditions pooled), and after
822 rhythmically inhibiting the head (blue, body coordinates 0-33), mid-body (orange, 33-66), or tail
823 (yellow, 66-99) neurons at 2 Hz. Rhythmic inhibition of the mid-body or tail increases the
824 frequency power at 1 Hz and decreases the power at the original undulation frequency,
825 mirroring (C). N≥16 trials per condition, with each worm supplying at most two trials. Shaded
826 outlines are the SEM. Vertical red lines indicate the imposed frequency (solid) or one-half of the
827 imposed frequency (dashed).
828
829 **Figure 9. A model for *C. elegans* forward locomotion**
830 Two units of the VNC motor neurons (and potentially more subsections) are capable of
831 independent rhythm generation. However, all oscillating units are coupled by proprioceptive
832 coupling (Wen et al., 2012) and another unknown, likely non-proprioceptive coupling
833 mechanism that allows signaling in the anteriorward direction, and potentially also in the
834 posteriorward direction. Pre-motor interneurons may activate or suppress this circuit, but are not
835 essential for rhythm generation or propagation.
836
837

838 **Figure 2 Figure Supplement 1. Tail undulation after gross head lesioning**

839 The approximate location of hot wire lesioning is indicated with a red arrow. Each panel
840 presents data from a different worm. Scale bars: 200 μm.

841 (A) Slow rhythmic undulations are evident posterior to the head.

842 (B) Rhythmic undulations in the mid-body arise after substantial damage is applied to the head.

843 (C) Rhythmic undulations in the neck and mid-body arise after substantial damage is applied to
844 the head.

845

846

847 **Figure 3 Figure Supplement 1. Additional disruptions to motor coupling cause 2FU**

848 (A) Two examples of worms in which all cholinergic neurons are inhibited (P*unc-17::NpHR*;
849 global yellow illumination) except for those within a small tail region (P*unc-17::ChR2*; blue
850 illumination in a small tail region). The A-type motor neurons were killed at the L2 larval stage
851 (P*unc-4::MiniSOG*). Green triangle: worm head; blue band: blue illumination region. The
852 curvature map (lower pane) indicates the spatiotemporal windows of yellow illumination (yellow
853 dotted box) and blue laser illumination (white dotted box). Scale bars: 200 μm.

854 (B) 2FU induced by an inhomogeneous mechanical environment. Red dotted line indicates the
855 boundary between low viscosity buffer (NGM) and high viscosity HPMC. Around t= 11s, the tail
856 continues oscillating at high frequency even as the head rapidly slows to a crawl inside the
857 HPMC.

858

859 **Figure 4 Figure Supplement 1. VNC premotor interneurons and several VNC motor**
860 **neuron classes are not required for de-synchronized oscillations.**

861 (A) 2FU occurs despite ablation of the premotor interneurons AVA, AVD, AVE, ,and PVC, and
862 other neurons (P*nmr-1::ICE*; P*myo-3::NpHR*). The spatiotemporal extent of green laser
863 illumination is indicated by the white dotted box.
864 (B) 2FU rarely occurs upon laser ablation of both AVB interneurons (See Figure 4 Figure
865 Supplement 2).
866 (C) Robust 2FU occurs despite ablation of the A- and C-type motor neurons (P*unc-4::MiniSOG*;
867 P*myo-3::NpHR*).
868 (D) *C. elegans vab-7* mutants, in which DB motor neurons are broadly disrupted, have
869 paralyzed tails and appear incapable of 2FU.
870 (E) When subjected to neck paralysis (P*myo-3::NpHR*), 2FU occurs reliably in P*nmr-1::ICE* and
871 P*unc-4::MiniSOG* animals, occasionally in *unc-7* animals, and rarely animals in which AVB has
872 been ablated. Each colored circle pair represents one trial; worms may have multiple trials (see
873 methods). N= 11, 8, 14, 16, and 19 worms per condition, respectively. Error boxes represent
874 mean and SEM. Head and mid-body data were measured at body coordinates 15 and 60,
875 respectively.
876 (F) Neck paralysis leads to modest decreases in tail bending amplitude in most conditions.
877
878
879

880 **Figure 4 Figure Supplement 2. Ablation of the AVB interneurons**

881 (A) Mock control with both AVB neurons visible (P*sra-11::D3cpv*). Yellow outline, worm pharynx.
882 Red arrows, AVB L/R in separate focal planes of the same worm. Yellow arrows, a pharyngeal
883 neuron, possibly I4. AVB cell bodies were identified by their placement at the medial anterior
884 edge of the terminal bulb of the pharynx, with processes directed ventrally. Scale bars: 50 μm.
885 (B) Worm in which both AVB interneurons were ablated at the L4 stage. Neither cell bodies nor
886 processes are visible. Behavioral recording of this worm is shown in Figure 4 Figure
887 Supplement 1.

888

889

890 **Figure 4 Figure Supplement 3. Subsets of B-type motor neurons are not required for 2FU**

891 Groups of 2-3 B-type motor neurons at a time were ablated using a pulsed infrared laser in
892 worms expressing P*myo-3::NpHR*; P*acr-2::wCherry*. See also Figure 4F.

893 (A) Curvature maps of worms that exhibited 2FU despite ablation of the indicated B-type motor
894 neurons and potentially some other neurons.

895 (B) wCherry fluorescence images of each worm to confirm cell death. Blue labels indicate some
896 or all B-type motor neurons. Red labels missing B-type neurons. White arrows indicate the
897 vulva. Scale bars: 100 μm.

898

899 **Figure 4 Figure Supplement 4. B-type motor neurons posterior to the vulva are not**
900 **required for 2FU**

901 We attempted to ablate all B-type motor neurons posterior to the vulva in worms expressing
902 P*myo-3::NpHR*; P*acr-2::wCherry*.

903 (A) Curvature maps of worms that exhibited 2FU despite ablation of the indicated B-type motor
904 neurons and potentially other neurons.

905 (B) wCherry fluorescence images of each worm to confirm cell death. Blue labels indicate some
906 or all B-type motor neurons. Red labels indicate missing B-type neurons. White arrows indicate
907 the vulva. Scale bars: 100 μm.

908

909 **Figure 4 Figure Supplement 5: Examples of 2FU occurrence prior to optogenetic**
910 **inhibition of neck muscles**

911 In some disruptions to the motor circuit, 2FU was observed occurring without inhibition of neck
912 muscles. Examples are shown here from an *unc-9* mutant (A), an *unc-7* mutant (B), an AVB-
913 ablated worm (C), and an *unc-49* mutant (D).

914

915 **Figure 5 Figure Supplement 1. Behavior after ablation of VB motor neurons**

916 Example curvature maps from trials in which 2FU was (A) and was not (B) observed after IR
917 laser ablation of VB motor neurons. VB3-VB11 were removed in both worms.

918

919 **Figure 6 Figure Supplement 1. Body undulations after severing the VNC and DNC do not**
920 **require the A motor neurons**

921 (A) Representative images of the VNC motor neurons in adult worms without (i) and with (ii)
922 illumination with blue light at the L2 larval stage. After illumination, only B and AS neurons were
923 visible along most of the body. In all worms tested however (N=20), at least one A motor neuron

924 was visible at the posterior end of the VNC, corresponding to either VA12, DA8, or DA9. The
925 behavior of the worm in (ii) is shown in C(i). Scale bars: 100 μm.

926 (B) Rhythmic waves visible posterior to the head after removal of the A motor neurons, severing
927 the VNC and DNC in the neck, and damaging the head.

928 (C) Rhythmic waves visible in the mid-body (i) and tail (ii) after removal of the A motor neurons,
929 severing the VNC and DNC in the neck, severing the VNC and DNC posterior to the vulva, and
930 damaging the head.

931

932 **Figure 6 Figure Supplement 2. B motor neurons are required for body undulations after**
933 **severing the VNC and DNC**

934 (A) Fluorescence image of the worm in (D), for which DB have been removed by MiniSOG and
935 VB have been removed by laser ablation. The remaining VA neurons and processes allow
936 visualization of the VNC, including the cut posterior to the pharynx (blue arrow). DA and DB
937 commissures are not visible. Scale bar: 100 μm.
938 (B-D) behavior during periods of mechanical vibration in worms for which the VNC and DNC
939 were severed posterior to the pharynx. Control worms exhibit robust undulation. Worms lacking
940 DB nearly always coiled in response to the stimulus, but in a minority of cases, very faint
941 movements, potentially oscillations, could be seen in the tip of the tail. Worms lacking DB and
942 VB also reacted to the stimulus by at least partially coiling, but rhythmic body undulations were
943 not observed.

944 (E) Recorded frequency during bouts of well-segmented non-reversal lasting at least two
945 seconds during periods of mechanical stimulation. Control worms routinely exhibited oscillations
946 in the mid-body and tail. DB ablated worms had no mid-body oscillations, but in one case

947 produced very faint high frequency tail oscillations (see C). DB and VB ablated worms lacked
948 any rhythmic oscillations. N = 58, 7, and 16 bouts from 15, 4, and 9 worms, respectively Mid-
949 body and tail frequency are measured at body coordinates 45 and 85, respectively.

950 (F) Subjective judgement worm behavior in each condition. Fractions indicate the number of
951 trials blindly scored as oscillating during 20 s periods of mechanical stimulus (anywhere along
952 the body) over the total number of trials. Oscillation was also not observed in DB or DB & VB
953 ablated worms outside periods of stimulus (not shown). Each animal was subjected to 1-2 such
954 stimulus trials. Error bars represent standard error of the sample proportion.

955 **Figure 8 Figure Supplement 1.** Rhythmic activity in the mid-body B motor neurons is sufficient
956 for posterior-to-anterior entrainment, and muscle-to-muscle gap junctions are not required.

957 (A) Representative kymogram from a P*acr-5::Arch* worm that was subject to rhythmic (1.7 Hz)
958 hyperpolarization of the mid-body B motor neurons (top), and average frequency spectra of the
959 head before and during rhythmic inhibition (bottom). Note an increase in amplitude at 0.85Hz,
960 one-half of the imposed frequency. N=22 trials were analyzed from 11 worms. Vertical red lines
961 indicate the imposed mid-body frequency (solid) or one-half of the imposed frequency (dashed).

962 (B) Equivalent analysis for worms in which the mid-body muscles were rhythmically inhibited
963 and muscle-to-muscle gap junctions are disrupted. Expression of UNC-9 in neurons was
964 transgenically restored (Wen et al., 2012). Note an increase in amplitude at 0.85 Hz, one half of
965 the imposed frequency. N=22 trials were analyzed from 11 worms.

966

967 **MATERIALS AND METHODS**

968 **Strains**

969 We maintained *C. elegans* on 6 cm NGM plates seeded with *E. coli* OP50 at 20˚C using
970 standard methods (Sulston and Hodgkin, 1988). For all optogenetic experiments, we added
971 100 mM all-*trans* retinal (ATR) in ethanol at 0.8% by volume to the bacteria suspension before
972 seeding the plates, and kept plates in darkness. All strains were synchronized by hypochlorite
973 bleaching and allowed to hatch on an NGM plate without food. L1 arrested larvae were
974 transferred to OP50 or OP50+ATR plates and allowed to grow to the appropriate stage. Unless
975 otherwise specified, all experiments were performed using day 1 adult hermaphrodites.

976 All strains used in this study are listed in Tables 1 and 2. All transgenic strains were outcrossed
977 a minimum of 3 times against N2.

978

979 **Table 1: Transgenic arrays acquired or generated for this study**

| Transgene | Plasmid or Reference | Description | Purpose | Strain |
|---|---|---|---|---|
| *vsIs48* | (Chase et al., 2004) | P*unc-17::GFP* | Identification of VNC and DNC | LX929 |
| *akIs11* | (Zheng et al., 1999) | P*nmr-1::ICE; lin-15(+)* | Ablation of INs | VM4770 |
| *kyIs36* | (Zheng et al., 1999) | P*glr-1::ICE; lin-15(+)* | Ablation of INs | VM4771 |
| *wenIs001* | pJH2918 | P*acr-5::ArchT::RFP; lin-15(+)* | Inhibition of B motor neurons | WEN001 |
| *qhIs1* | (Leifer et al., 2011; Husson et al., 2012) | P*myo-3::NpHR::ECFP; lin-15(+)* | Inhibition of muscles | YX9 |
| *qhIs2* | | | | YX10 |
| *qhIs4* | pJH1841 | P*acr-2::wCherry; dpy-20(+)* | Identification of B | YX146 |
| *qhIs5* | (Xu and Chisholm, 2016) | P*myo-3::PH::miniSOG(Q103L)* + P*myo-3::mCherry* + P*ttx-3::RFP* | Ablation of BWM | YX203 |
| *qhIs9* | (Xu and Chisholm, 2016) | P*unc-17(beta)::PH::miniSOG (Q103L)*+ P*acr-2::mCherry*+ P*ttx-3::RFP* | Ablation of B | YX234 |
| *hpEx803* | (Wen et al., 2012) | *unc-9(fc16); hpIs3;* P*rgef-1-unc-9cDN) + odr-1* | Neuronal *unc-9* rescue | ZM2509 |
| *zxIs6* | (Liewald et al., 2008) | P*unc-17::ChR2(H134R)::YFP; lin-15(+)* | Stimulation of cholinergic neurons | ZX460/ ZM3265 |
| *hpIs166* | (Gao et al., 2015) | P*glr-1::chop-2(H134R)::YFP; lin-15(+)* | Identification of INs | ZM4624 |
| *hpIs178* | (Leifer et al., 2011) | P*unc-17::NpHR::ECFP; lin-15(+)* | Inhibition of cholinergic neurons | ZM5016 |
| *hpIs179* | (Kawano et al., 2011) | P*sra-11::D3cpv* | Identification of AVB | ZM5132 |
| *hpIs366* | pJH2843 | P*unc-4::tomm-20::miniSOG:: urSL::wCherry; lin-15(+)* | Ablation of A and VC | ZM7690 |
| *hpIs371* | | | | ZM7691 |

980

981

982 **Table 2: Additional strains generated by combining transgenes in Table 1**

| Strain | Transgenes | Description | Purpose |
|---|---|---|---|
| YX119 | *qhIs1; unc-49(e407)* | Muscle::NpHR, *unc-49* | 2FU with D function impaired |
| YX126 | *qhIs1; hpIs371* | Muscle::NpHR, A/VC::miniSOG | 2FU with A and VC removed |
| YX127 | *hpIs178; hpIs371; zxIs6* | Cholinergic Neurons::NpHR&ChR2, A/VC::miniSOG | Inhibition or excitation of Cholinergic neurons with A removed |
| YX135 | *qhIs1; vab-7(e1562) III.* | Muscle::NpHR, DB disrupted | 2FU (fails) with DB disrupted |
| YX137 | *qhIs1; unc-7(e5)* | Muscle::NpHR, *unc-7* | 2FU with AVB::B gap junctions disrupted |
| YX139 | *qhIs1; unc-9(fc16); hpEx803* | Muscle::NpHR, UNC-9 disruption in muscles only | Entrainment with BWM::BWM gap junctions disrupted |
| YX140 | *qhIs1; unc-9(fc16)* | Muscle::NpHR, *unc-9* | 2FU with AVB::B gap junctions disrupted |
| YX148 | *qhIs1; qhIs4* | Muscle::NpHR, AB::RFP | 2FU with some B removed OR undulation with nerve cords severed |
| YX152 | *hpIs166; akIs11* | IN::ICE&YFP | Assessment of ICE ablations |
| YX153 | *hpIs166; kyIs36* | IN::ICE&YFP | Assessment of ICE ablations |
| YX159 | *qhIs2; akIs11* | Muscle::NpHR, IN::ICE | 2FU with PVC removed |
| YX160 | *qhIs2; kyIs36* | Muscle::NpHR, IN::ICE | 2FU with PVC removed |
| YX177 | *hpIs366; vsIs48* | A/VC::miniSOG, Cholinergic Neurons::GFP | Undulation with nerve cords severed and A removed. |
| YX223 | *qhIs1; qhIs9* | Muscle::NpHR, DB ablated | 2FU with B removed OR undulation with nerve cords severed and B removed. |
| YX230 | *qhIs1; hpIs179* | Muscle::NpHR, AVB labeled for ablation | 2FU with AVB removed |

983

984 **Construction and validation of the optogenetic targeting system**

985 We constructed an optogenetic targeting system similar to that described in Leifer et al (2011)
986 based around a Leica DMI4000B microscope. Dark field illumination was provided by red LEDs
987 and worms were imaged with a sCMOS camera (QImaging optiMOS). Custom written C++
988 software performs image segmentation of the worm and allows the user to select a region of the
989 worm to illuminate. The illumination region is sent to a digital micromirror device (DMD), which

990 then projects the laser onto only the desired portion of the worm through a 10X objective. The
991 entire cycle runs at 40 Hz. A green laser (Shanghai Laser & Optics Century GL532T3-300, 532
992 nm wavelength, irradiance 10 mW/mm$^2$ at focal plane) was used for all activations of NpHR or
993 Arch, and a blue laser (Shanghai Laser & Optics Century BL473T3-150, 473 nm wavelength,
994 irradiance 4 mW/mm$^2$ at focal plane) was used for activation of ChR2. Worms were placed in a
995 solution of 17% dextran in NGMB (Fang-Yen et al., 2010) in an 80 μm thick chamber between a
996 microscope slide and cover glass, separated by glass beads. NGMB is identical to NGM
997 (Stiernagle, 2006) but without agar, peptone, or cholesterol.

998 To determine the accuracy of our illumination system, we studied worms expressing the
999 excitatory opsin ChR2 under the control of the *aptf-1* promoter. These worms were reported to
1000 quickly become quiescent when the RIS head neuron is illuminated with blue light (Turek et al.,
1001 2013). We targeted a thin band of blue light to various locations along the centerline of each
1002 worm, and measured the amplitude of head bending waves as an output (data not shown). The
1003 distance between the region where most slowing occurred (body coordinate 14) and the nearest
1004 region with no slowing (body coordinate 20) suggests that our optogenetic targeting system has
1005 a resolution of about 6% of an adult worm's body length, similar to that reported for a previous
1006 system (Leifer et al., 2011).

1007 **Optogenetic inhibition and stimulation**

1008 For head and neck optogenetic inhibition experiments, YX9 (Muscle::NpHR), ZM5016
1009 (Cholinergic Neurons::NpHR), WEN001 (B::Arch) , YX127 (Cholinergic Neurons::NpHR&ChR2,
1010 A/VC::miniSOG), YX119 (Muscle::NpHR, *unc-49*(*e407*)), YX135 (Muscle::NpHR, *vab-7(e1562),*
1011 YX137 (Muscle::NpHR, *unc-7*(*e5*)), or YX140 (Muscle::NpHR, *unc-9*(*fc16*)) larvae were
1012 transferred to ATR plates and allow to grow to first day of adulthood. Up to 20 adult worms were
1013 mounted at a time on our optogenetic targeting system. Worms were sampled with replacement

1014 from the dextran chamber, and illuminated with a green (532 nm wavelength) laser a total of 1-3
1015 times in the indicated region, with at least 10 s between successive illuminations of the same
1016 animal.

1017 For activation of posterior B and AS motor neurons, YX127 (Cholinergic neurons::NpHR&ChR2,
1018 A/VC::miniSOG) worms were allowed to grow to the second larval stage on ATR plates, and
1019 then illuminated *en masse* with blue light (470 ± 17 nm wavelength) at 3 mW/mm$^2$ for 20
1020 minutes to ablate the A-type motor neurons. Worms were transferred to a fresh ATR plate to
1021 grow for 2 more days. To confirm a loss of reversal capability in each day 1 adult, worms were
1022 individually prodded with a platinum wire worm pick. All worms tested failed to move backwards
1023 during this assay. Worms were then mounted on the optogenetic targeting system as before.
1024 Global amber (580 ± 15 nm wavelength) illumination was applied through the transmitted light
1025 port of the microscope and varied in irradiance until just strong enough to paralyze the worm,
1026 presumably through the action of P*unc-17::NpHR*. Once paralyzed or nearly paralyzed, 473 nm
1027 laser light was applied to the indicated region of the tail using the DMD.

1028 For rhythmic inhibition of muscles or cholinergic neurons, synchronized YX148 (Muscle::NpHR,
1029 AB::RFP) L4 larvae, YX139 (Muscle::NpHR, BWM gap junctions disrupted) L4 larvae, YX127
1030 day 1 adults, or WEN001, day 1 adults grown on ATR plates were mounted on the optogenetic
1031 targeting system and illuminated periodically at the indicated frequency and location through our
1032 custom software. For this experiment, L4 *qhIs1* larvae were used because expression of *myo-*
1033 *3::NpHR::ECFP* in the BWMs appeared to be weaker in adults. YX127 animals were not
1034 exposed to blue light prior to this experiment.

1035 **Neuron and muscle photoablation using miniSOG**

1036 For optogenetic 2FU experiments, YX126 (Muscle::NpHR, A/VC::miniSOG) larvae were allowed
1037 to grow for 2 days on OP50 plates until the L4 stage, at which RFP was visible in the both the A-

1038 and VC-type motor neurons. Worms were bulk illuminated with blue light (wavelength 470±17
1039 nm) at 3.5 mW/mm$^2$ for 20 minutes of total illumination time using 0.5 s on / 1.5 s off pulse train
1040 (Qi et al., 2012) from a Leica EL6000 light source. After illumination, the larvae were transferred
1041 to OP50+ATR plates and incubated for 2 additional days, but did not appear to grow past the L4
1042 stage. During the optogenetic experiments, worms were observed swimming forward and
1043 stopping, but never in reverse. In addition, worms were handled individually and recovered from
1044 the dextran chamber for fluorescence imaging. We mounted each worm on a separate 4% agar
1045 pad and acquired RFP images on a compound fluorescence microscope (Leica DMI6000B). In
1046 control worms, which grew into adults, RFP was visible in the VC-type motor neurons, some A-
1047 type motor neurons (RFP was visible in all A-type motor neurons at the L2-L4 stages), and the
1048 posterior intestine. The normal RFP expression pattern in A- and VC-type motor neuron was
1049 absent in all illuminated worms. However, neurons in the tail corresponding to VA12, DA8, or
1050 DA9 were usually visible (see also Figure 6 - Figure Supplement 1A).

1051 For VNC/DNC cauterization experiments, YX177 (AB::RFP, A/VC::miniSOG) worms were
1052 exposed to blue light at the L2 stage using 0.5 s on / 1.5 s off pulsing and surgically manipulated
1053 at the day 2 adult stage as described below. Ablation of the A motor neurons was assessed by
1054 recording GFP fluorescence images of each animal after behavioral imaging. In all animals, only
1055 B and AS motor neurons were visible along most of the VNC, with the exception of the three
1056 posterior A motor neurons noted above.

1057 For body wall muscle ablation experiments, YX203 (BWM::miniSOG) adults were immobilized
1058 on agar pads using polystyrene beads (Kim et al., 2013) and the indicated region of the body
1059 was exposed to light with wavelength 470 ± 20 nm at an irradiance of 75 mW/mm$^2$ through a
1060 40x objective on a Leica DMI6000B or DMI4000B microscope for 5.5 minutes with a 0.5 s on /
1061 0.5 s off pulse protocol (Xu and Chisholm, 2016). Spatial selectivity was achieved by restricting
1062 the diameter of illumination by adjusting the microscope's epifluorescence field diaphragm. After

1063 illumination, worms were recovered to an unseeded plate and immediately transferred to a 17%
1064 dextran chamber for behavioral imaging.

1065 For B ablation experiments using P*unc-17::PH::miniSOG* (YX223), we found that illumination at
1066 any larval stage preferentially killed the DA and DB motor neurons, but left most VA and VB
1067 alive, as determined by the loss of all dorsal commissures and DNC labeling by P*acr-*
1068 *2::mCherry* (not shown). Hence, we illuminated all YX223 animals at the L1 stage for 20
1069 minutes with 0.25 s on / 0.25 s off pulsing (Xu and Chisholm, 2016) to kill DB. Worms were
1070 recovered to ATR (for optogenetic 2FU) or regular seeded (for VNC surgery) plates. Additional
1071 laser ablation of VB neurons was performed at the L4 stage, and lesioning of the VNC and DNC
1072 was performed at the day 2 adult stage (both described below).

1073

1074 **Ablation of premotor interneurons by ICE**

1075 Prior to conducting optogenetic experiments, we generated strains YX152 (P*nmr-1::ICE*; P*glr-*
1076 *1::ChR2::YFP*) and YX153 (P*glr-1::ICE*; P*glr-1::ChR2::YFP*) to test whether the interneurons
1077 were appropriately ablated. Control ZM4624 (P*glr-1*::ChR2::YFP) L1 larvae and adults showed
1078 bright YFP labeling of many neurons, including many head neurons and PVC, the only pair of
1079 labeled neurons in the tail.

1080 In L1 arrested YX152 and YX153 worms, many neurons were also easily visualized by YFP,
1081 although normal locomotion was impaired. By the adult stage, YFP signals in all head and tail
1082 neurons had nearly vanished in all YX153 worms (N=18); some small and faint fluorescent
1083 puncta, similar in appearance to intestinal birefringent granules, were visible in the nerve ring
1084 and tail. These dim puncta did not have visible processes, and we were unable to identify any
1085 head neurons or PVC in any of these worms. In YX152 adults, PVC was similarly not identifiable
1086 in any worm (N=10), although many brightly YFP-labeled neurons were visible in the nerve ring.

1087 These results suggest that all or most P*glr-1* positive interneurons are ablated in P*glr-1*::ICE
1088 worms and that PVC (and likely other P*nmr-1* positive neurons) are ablated in P*nmr-1::ICE*
1089 worms. AVB are likely present in both P*glr-1::ICE* and P*nmr-1::ICE* worms. (Kawano et al.,
1090 2011; Kawano, Po, and Zhen, unpublished).

1091 For optogenetic experiments, we generated strains YX159 (Muscle::NpHR, IN::ICE) and YX160
1092 (Muscle::NpHR, IN::ICE) and performed optogenetic illuminations as in our original optogenetic
1093 2FU experiments.

1094

1095 **Pulsed infrared laser cauterization of neurons and nerve cords**

1096 For ablation of B motor neurons or AVB interneurons, YX148 (Muscle::NpHR, AB::RFP), YX223
1097 (Muscle::NpHR, DB killed by miniSOG, see above), or YX230 (Muscle::NpHR, AVB labeled)
1098 worms were raised on ATR plates until most animals were at the L3 to L4 stage, and then
1099 immobilized on 4-10% agar pads using 50 nm polystyrene beads (Kim et al., 2013). Each pad
1100 was mounted on a pulsed infrared laser system (Churgin et al., 2013) that had been modified
1101 with increased power to deliberately kill cells. Each neuron, visualized by RFP or GFP
1102 fluorescence optics, was irradiated with a single 0.8 to 1.6 ms pulse of the 400 mW laser
1103 through a 63X oil immersion objective. We determined that a single 0.8 ms pulse reliably kills a
1104 targeted VNC motor neuron, has a 50% chance of killing a VNC neighbor within 2.5 μm, and
1105 has a 10% chance of killing a VNC neighbor within 5 μm from the target (A. D. F. and C. F.-Y.,
1106 unpublished data). After ablation, worms were recovered and transferred to a fresh ATR plate to
1107 resume development for 1 additional day. During optogenetic experiments, worms were handled
1108 individually and recovered to agar pads after illumination.

1109 To sever the VNC and DNC, day 2 adult YX148 or LX929 (Cholinergic neuron::GFP) worms
1110 were immobilized with polystyrene beads and mounted on our infrared laser system as before,

1111 and the indicated area of the wCherry- or GFP-labeled cord was illuminated with a train of 10-25
1112 IR laser pulses with 2 ms duration. Worms were transferred to fresh unseeded plates and
1113 allowed to recover for at least four hours before behavioral and fluorescence imaging. For
1114 behavioral imaging, worms were mounted individually in 20% dextran chambers and recorded
1115 swimming for at least 1 minute under dark field illumination. Most worms were inactive 4 hours
1116 after surgery, especially when the VNC and DNC were lesioned in two locations (not shown).

1117 In many other systems, mechanical, electrical, or chemical stimuli can be applied to induce
1118 swimming or fictive swimming in an otherwise quiescent preparation (Kristan et al., 2005). To
1119 agitate *C. elegans,* we mechanically vibrated each worm using a 200 Hz cell phone motor for
1120 periods of 10-20 s to induce locomotion at least twice during each recording. After behavioral
1121 imaging, each worm was transferred to a pad and imaged for red or green fluorescence
1122 imaging.

1123 **Fluorescence imaging and identification of neurons and nerve cord lesions**

1124 For all neuron ablation or nerve cord lesioning experiments, we acquired RFP or GFP
1125 fluorescence images of each animal through a 40X objective on a compound fluorescence
1126 microscope (Leica DMI 6000B). Through examination of images, A and B type motor neurons or
1127 AVB interneurons were labeled as present or missing based on the location, stereotypic
1128 ordering, commissural orientation, and the presence or absence of commissures from dorsal A-
1129 or B-type motor neurons. In ablation conditions labeled “most VB” in Figure 5 and Figure 6
1130 Figure Supplement 2, we only used data from animals in which at most 3 out of the 9 VB
1131 neurons between VB3 and VB11 inclusive were visible. In DB ablation conditions in the same
1132 two figures, all DB motor neurons appeared to be missing, and occasionally some VA/VB were
1133 missing as well. However, we generally could not identify B motor neurons anterior to VB3
1134 because of clustering and the presence of very bright AIY::RFP in *qhIs9*. In each category in

1135 Figure 4F, we included only worms for which all indicated B motor neurons were missing. Some
1136 individuals in each category had additional missing neurons. In Figure 4 – Figure Supplements
1137 3 and 4, all ablated B motor neurons are indicated for each individual worm example. In AVB
1138 ablation conditions, we only analyzed data from worms in which both AVB cell bodies and their
1139 associated processes were removed. Because cell killing occurs over a ~3 μm radius volume in
1140 our system, it is highly likely that other head neurons were also damaged or killed by this
1141 procedure. For nerve cord lesioning experiments, we only analyzed data from animals in which
1142 all indicated VNC/DNC targets were clearly severed.

1143

1144

1145 **Head lesions using a heated wire**

1146 To broadly lesion the head and inhibit anterior bending, four freely crawling adult N2 worms
1147 were gently touched on or near the head with a platinum wire attached to a soldering iron. The
1148 worms appeared to crawl backwards after the initial touch, so we applied a second touch to the
1149 agar near the tail to induce forward locomotion. We recorded behavior immediately after
1150 lesioning.

1151

1152

1153 **Heterogenous mechanical environment experiments**

1154 Day 1 adult N2 worms were transferred to a slide containing 3 to 5 μL islands of solutions of
1155 high viscosity 3% hydroxypropylmethylcellulose (HPMC, Ashland Benecel K200M) in NGMB,
1156 surrounded by NGMB without HPMC. A second slide, spaced by 125 μm thick plastic spacers,
1157 was placed on top to form a 2-dimensional chamber similar to those used for optogenetics
1158 experiments, but with an inhomogeneous mechanical environment. We imaged each slide

1159 under dark field illumination on a Nikon TE2000-S microscope and recorded worms transitioning
1160 from low viscosity to high viscosity regions.

1161

1162 **Curvature segmentation, analysis, and statistics**

1163 For experiments with our optogenetic targeting system, the real-time segmentation for body
1164 targeting was recorded to disk along with each video frame. We wrote custom MATLAB codes
1165 to compute the curvature of the worm in each frame using the recorded centerline coordinates.
1166 All analysis codes, codes for the optogenetic targeting system, and source data for figures are
1167 freely available (Fouad et al., 2017). Frequencies and amplitudes in optogenetic experiments
1168 were measured over either a 3 s non-illuminated interval ending at the start of illumination, or a
1169 3 s illuminated interval beginning at the start of illumination. Trials were excluded if, during the
1170 period of analysis, (1) the worm showed reverse locomotion at any time, or (2) the segmentation
1171 algorithm was disrupted, for example if the worm touched a bubble, another worm, or the edge
1172 of the chamber.

1173 For all other experiments, worm segmentations were generated from dark field videos using
1174 WormLab software (MBF Bioscience, Williston, VT). The centerline coordinates were exported
1175 and curvature maps constructed as before. To identify bouts of forward locomotion in 1-2 min
1176 worm recordings, we computed the activity level and wave direction in the kymogram as a
1177 function of time and body coordinate. Bouts of forward locomotion in body segments were
1178 identified when the activity level was higher than a fixed threshold and the local direction of
1179 wave propagation was anterior-to-posterior for longer than the amount of time specified
1180 (typically 2-3 s).

1181 To measure frequencies of undulation at any body coordinate, we computed the Fourier
1182 transform of time derivative of the curvature, and identified the frequency corresponding to the

maximum amplitude within a 0 to 2.5 Hz window. For trials in which no clear peak emerged (i.e. the maximum amplitude was less than a fixed threshold), no undulations were considered to have occurred and the frequency was treated as zero. The same threshold was used for every frequency measurement presented. In ratiometric measurements, a small number (<2%) of ratios with infinite values were excluded. Bending amplitudes were calculated as the root mean square of time differentiated curvature. Changes in the mean frequency, frequency ratio, or bending amplitude of all paired data were evaluated using a paired t-test.

For blinded, randomized scoring of trials shown in Figure 5 and Figure 6 Figure Supplement 2, kymograms were scored manually without prior examination of the data. Trials were scored as “2FU” or “oscillating” if the following criteria were met: (1) bending waves were visible in the tail that did not appear to arise from the head, and (2) at least two complete undulatory cycles occurred in the tail, in any portion of the optogenetic inhibition or vibration stimulus time windows, which were 8 and 20 seconds, respectively. Trials were marked for exclusion if the windows contained exclusively reversal or incorrectly segmented behavior. The manual scoring method allowed detection of 2FU occurring outside the 3 second window used for quantitative analysis, which is why more 2FU trials were found in the DB ablation condition by manual scoring than by quantitative frequency analysis.

1202 **VIDEO TITLES**

1203 **Video 1:** Posterior undulations after optogenetic inhibition of anterior body wall muscles or
1204 cholinergic neurons

1205 **Video 2:** Two-frequency undulation during optogenetic inhibition of neck BWM, cholinergic
1206 neurons, or B motor neurons.

1207 **Video 3:** Additional manipulations that evoke two-frequency undulation (2FU): Stimulation of B
1208 and AS during tail paralysis; inhomogenous mechanical environment.

1209 **Video 4:** Removal of B motor neurons by miniSOG and laser ablation eliminates 2FU.

1210 **Video 5:** Posterior undulations occur after severing the ventral and dorsal nerve cords with an
1211 infrared laser (VNC-isolated animals).

1212 **Video 6**: Removal of B motor neurons by miniSOG and laser ablation eliminates undulations in
1213 VNC-isolated animals.

1214 **Video 7:** Head undulation frequency can be entrained by rhythmic mid-body optogenetic
1215 manipulation of the muscles or cholinergic neurons.

1216

1217

1218 **ACKNOWLEDGEMENTS**

1219 We thank Mei Zhen, Quan Wen, Min Wu, Michelle Po, Yishi Jin, Andres Villu Mariq, and
1220 Alexander Gottschalk for providing strains. Some strains were provided by the by the CGC,
1221 which is funded by NIH Office of Research Infrastructure Programs (P40 OD010440). C. F.-Y.
1222 was supported by the National Institutes of Health, Ellison Medical Foundation, and Sloan
1223 Research Foundation. A. D. F. was supported by the National Institutes of Health. S. T. was
1224 supported by an Abraham Noordergraaf Research Fellowship and a Littlejohn Fellowship. J. R.
1225 M. was supported by a Holtz Undergraduate Research Fellowship. We thank Mei Zhen,
1226 Michael Nusbaum, David Raizen, Vijay Balasubramanian, Robert Kalb, Gal Haspel, Brian
1227 Chow, and Edward Fouad for helpful suggestions and discussions, Matthew Churgin for
1228 technical assistance, and Wassana Techadilok for assistance with figure preparation.

1229

1230 **REFERENCES**


1231 Ahringer, J. (2006). Reverse Genetics. In WormBook.

1232 Altun, Z.F., and Hall, D.H. (2011). Nervous system, general description. In WormAtlas.

1233 Andersson, O., Forssberg, H., Grillner, S., and Wallén, P. (1981). Peripheral feedback mechanisms acting
1234 on the central pattern generators for locomotion in fish and cat. Canadian Journal of Physiology and
1235 Pharmacology 59, 713-726.

1236 Bamber, B.A., Beg, A.A., Twyman, R.E., and Jorgensen, E.M. (1999). The Caenorhabditis elegans
1237 unc-49 Locus Encodes Multiple Subunits of a Heteromultimeric GABA Receptor. The Journal of
1238 Neuroscience 19, 5348-5359.

1239 Berri, S., Boyle, J.H., Tassieri, M., Hope, I., and Cohen, N. (2009). Forward locomotion of the nematode C.
1240 elegans is achieved through modulation of a single gait. HFSP Journal 3, 186-193.

1241 Boyle, J.H., Berri, S., and Cohen, N. (2012). Gait modulation in C. elegans: an integrated neuromechanical
1242 model. Frontiers in Computational Neuroscience 6, 10.

1243 Brockie, P.J., and Maricq, A.V. (2006). Ionotropic glutamate receptors: genetics, behavior and
1244 electrophysiology. In WormBook, T.C.e.R. Community, ed.

1245 Chalfie, M., Sulston, J., White, J., Southgate, E., Thomson, J., and Brenner, S. (1985). The Neural Circuit
1246 for Touch Sensitivity in Caenorhabditis elegans. The Journal of Neuroscience 5, 956-964.

1247 Chase, D.L., and Koelle, M.R. (2007). Biogenic amine neurotransmitters in C. elegans. In WormBook, The
1248 C. elegans Research Community, ed.

1249 Chase, D.L., Pepper, J.S., and Koelle, M.R. (2004). Mechanism of extrasynaptic dopamine signaling in
1250 *Caenorhabditis elegans*. Nat Neurosci 7, 1096-1103.

1251 Churgin, M.A., He, L., Murray, J.I., and Fang-Yen, C. (2013). Efficient Single-Cell Transgene Induction in
1252 Caenorhabditis elegans Using a Pulsed Infrared Laser. G3: Genes|Genomes|Genetics 3, 1827-1832.

1253 Cohen, A.H. (1987). Intersegmental coordinating system of the lamprey central pattern generator for
1254 locomotion. Journal of Comparative Physiology A 160, 181-193.
1255 Duerr, J.S., Han, H.P., Fields, S.D., and Rand, J.B. (2008). Identification of major classes of cholinergic
1256 neurons in the nematode Caenorhabditis elegans. The Journal of comparative neurology 506, 398-408.
1257 Evans, T.C. (2006). Transformation and microinjection. WormBook.
1258 Fang-Yen, C., Alkema, M.J., and Samuel, A.D.T. (2015). Illuminating neural circuits and behaviour in
1259 <em>Caenorhabditis elegans</em> with optogenetics. Philosophical Transactions of the
1260 Royal Society B: Biological Sciences 370.
1261 Fang-Yen, C., Wyart, M., Xiea, J., Kawaia, R., Kodgere, T., Chena, S., Wen, Q., and Samuel, A.D.T. (2010).
1262 Biomechanical analysis of gait adaptation in the nematode Caenorhabditis elegans. Proceedings of the
1263 National Academy of Sciences 107, 20323–20328.
1264 Flytzanis, N.C., Bedbrook, C.N., Chiu, H., Engqvist, M.K.M., Xiao, C., Chan, K.Y., Sternberg, P.W., Arnold,
1265 F.H., and Gradinaru, V. (2014). Archaerhodopsin Variants with Enhanced Voltage Sensitive Fluorescence
1266 in Mammalian and Caenorhabditis elegans Neurons. Nature communications 5, 4894-4894.
1267 Fouad, A., Teng, S., Mark, J.R., Liu, A., Alvarez-Illera, P., Ji, H., Du, A., Bhirgoo, P.D., Cornblath, E., Guan,
1268 A.*, et al.* (2017). Data from: Distributed rhythm generators underlie Caenorhabditis elegans forward
1269 locomotion. Dryad Digital Repository, ed. https://doi.org/10.5061/dryad.q0d1n
1270 Friesen, W.O., and Hocker, C.G. (2001). Functional Analyses of the Leech Swim Oscillator. Journal of
1271 Neurophysiology 86, 824.
1272 Gao, S., Guan, S.A., Fouad, A.D., Meng, J., Kawano, T., Huang, Y.-C., Li, Y., Alcaire, S., Hung, W., Lu, Y.*, et*
1273 *al.* (2017). Excitatory motor neurons are local oscillators for reverse locomotion. eLife 6, e29915.
1274 Gao, S., Xie, L., Kawano, T., Po, M.D., Pirri, J.K., Guan, S., Alkema, M.J., and Zhen, M. (2015). The NCA
1275 sodium leak channel is required for persistent motor circuit activity that sustains locomotion. Nat
1276 Commun 6.

1277 Gjorgjieva, J., Biron, D., and Haspel, G. (2014). Neurobiology of Caenorhabditis elegans Locomotion:
1278 Where Do We Stand? BioScience 64, 476-486.
1279 Goulding, M. (2009). Circuits controlling vertebrate locomotion: moving in a new direction. Nature
1280 Reviews Neuroscience 10, 507-518.
1281 Grillner, S., and El Manira, A. (2015). The intrinsic operation of the networks that make us locomote.
1282 Current Opinion in Neurobiology 31, 244-249.
1283 Grillner, S., McClellan, A., and Perret, C. (1981). Entrainment of the spinal pattern generators for
1284 swimming by mechano-sensitive elements in the lamprey spinal cord in vitro. Brain Research 217, 380-
1285 386.
1286 Haspel, G., O'Donovan, M.J., and Hart, A.C. (2010). Motorneurons dedicated to either forward or
1287 backward locomotion in the nematode C. elegans. The Journal of neuroscience : the official journal of
1288 the Society for Neuroscience 30, 11151-11156.
1289 Husson, S.J., Liewald, J.F., Schultheis, C., Stirman, J.N., Lu, H., and Gottschalk, A. (2012). Microbial Light-
1290 Activatable Proton Pumps as Neuronal Inhibitors to Functionally Dissect Neuronal Networks in C.
1291 elegans. PLoS ONE 7, e40937.
1292 Jorgensen, E.M. (2005). GABA. In WormBook, WormBook, ed. (The C. elegans Research Community).
1293 Karbowski, J., Schindelman, G., Cronin, C., Seah, A., and Sternberg, P. (2008). Systems level circuit model
1294 of C. elegans undulatory locomotion: mathematical modeling and molecular genetics. J Comput
1295 Neurosci 24, 253-276.
1296 Kawano, T., Po, Michelle D., Gao, S., Leung, G., Ryu, William S., and Zhen, M. (2011). An Imbalancing Act:
1297 Gap Junctions Reduce the Backward Motor Circuit Activity to Bias C. elegans for Forward Locomotion.
1298 Neuron 72, 572-586.
1299 Kerr, R. (2006). Imaging the activity of neurons and muscles. WormBook, ed. (The C. elegans Research
1300 Community).

1301 Kerr, R., Lev-Ram, V., Baird, G., Vincent, P., Tsien, R.Y., and Schafer, W.R. (2000). Optical Imaging of
1302 Calcium Transients in Neurons and Pharyngeal Muscle of C. elegans. Neuron 26, 583-594.
1303 Kiehn, O. (2006). Locomotor circuits in the mammalian spinal cord. Annual Review of Neuroscience 29,
1304 279-306.
1305 Kiehn, O. (2016). Decoding the organization of spinal circuits that control locomotion. Nat Rev Neurosci
1306 17, 224-238.
1307 Kim, E., Sun, L., Gabel, C.V., and Fang-Yen, C. (2013). Long-Term Imaging of Caenorhabditis elegans Using
1308 Nanoparticle-Mediated Immobilization. PLoS ONE 8, e53419.
1309 Kocabas, A., Shen, C.-H., Guo, Z., and Ramanathan, S. (2012). Controlling interneuron activity in
1310 Caenorhabditis elegans to evoke chemotactic behaviour. Nature 490, 273-278.
1311 Kristan, W.B., Calabrese, R.L., and Friesen, W.O. (2005). Neuronal control of leech behavior. Progress in
1312 Neurobiology 76, 279-327.
1313 Lai, C.-H., Chou, C.-Y., Ch'ang, L.-Y., Liu, C.-S., and Lin, W.-c. (2000). Identification of Novel Human Genes
1314 Evolutionarily Conserved in Caenorhabditis elegans by Comparative Proteomics. Genome Research 10,
1315 703-713.
1316 Leifer, A.M., Fang-Yen, C., Gershow, M., Alkema, M.J., and Samuel, A.D.T. (2011). Optogenetic
1317 manipulation of neural activity in freely moving Caenorhabditis elegans. Nat Meth 8, 147-152.
1318 Liewald, J.F., Brauner, M., Stephens, G.J., Bouhours, M., Schultheis, C., Zhen, M., and Gottschalk, A.
1319 (2008). Optogenetic analysis of synaptic function. Nat Meth 5, 895-902.
1320 Liu, P., Chen, B., Mailler, R., and Wang, Z.-W. (2017). Antidromic-rectifying gap junctions amplify
1321 chemical transmission at functionally mixed electrical-chemical synapses. Nature Communications 8,
1322 14818.
1323 Liu, Q., Chen, B., Gaier, E., Joshi, J., and Wang, Z.W. (2006). Low conductance gap junctions mediate
1324 specific electrical coupling in body-wall muscle cells of Caenorhabditis elegans. J Biol Chem 281.

1325 Marder, E., and Bucher, D. (2007). Understanding Circuit Dynamics Using the Stomatogastric Nervous
1326 System of Lobsters and Crabs. Annual Review of Physiology 69, 291-316.
1327 Marder, E., Bucher, D., Schulz, D.J., and Taylor, A.L. (2005). Invertebrate Central Pattern Generation
1328 Moves along. Current Biology 15, R685-R699.
1329 Marder, E., and Calabrese, R.L. (1996). Principles of rhythmic motor pattern generation. Physiological
1330 Reviews 76, 687-717.
1331 McClellan, A.D., and Sigvardt, K.A. (1988). Features of entrainment of spinal pattern generators for
1332 locomotor activity in the lamprey spinal cord. The Journal of Neuroscience 8, 133.
1333 McIntire, S., Jorgensen, E., and Horvitz, H. (1993a). Genes required for GABA function in Caenorhabditis
1334 elegans. Nature 364, 334-337.
1335 McIntire, S., Jorgensen, E., Kaplan, J., and Horvitz, H. (1993b). The GABAergic nervous system of
1336 Caenorhabditis elegans. Nature 364, 337-341.
1337 Mullins, O.J., Hackett, J.T., Buchanan, J.T., and Friesen, W.O. (2011). Neuronal control of swimming
1338 behavior: Comparison of vertebrate and invertebrate model systems. Progress in Neurobiology 93, 244-
1339 269.
1340 Nagel, G., Brauner, M., Liewald, J.F., Adeishvili, N., Bamberg, E., and Gottschalk, A. (2005). Light
1341 Activation of Channelrhodopsin-2 in Excitable Cells of Caenorhabditis elegans Triggers Rapid Behavioral
1342 Responses. Current Biology 15, 2279-2284.
1343 Pearce, R.A., and Friesen, W.O. (1985). Intersegmental coordination of the leech swimming rhythm. I.
1344 Roles of cycle period gradient and coupling strength. Journal of Neurophysiology 54, 1444.
1345 Pierce-Shimomura, J.T., Chen, B.L., Mun, J.J., Ho, R., Sarkis, R., and McIntire, S.L. (2008). Genetic analysis
1346 of crawling and swimming locomotory patterns in C. elegans. Proceedings of the National Academy of
1347 Sciences 105, 20982-20987.

1348 Qi, Y.B., Garren, E.J., Shu, X., Tsien, R.Y., and Jin, Y. (2012). Photo-inducible cell ablation in
1349 Caenorhabditis elegans using the genetically encoded singlet oxygen generating protein miniSOG.
1350 Proceedings of the National Academy of Sciences 109, 7499-7504.
1351 Rand, J.B. (2007). Acetylcholine. In WormBook, The C. elegans Research Community, ed.
1352 Robertson, R.M., and Pearson, K.G. (1983). Interneurons in the flight system of the locust: Distribution,
1353 connections, and resetting properties. The Journal of comparative neurology 215, 33-50.
1354 Rotstein, H.G., Schneider, E., and Szczupak, L. (2017). Feedback Signal from Motoneurons Influences a
1355 Rhythmic Pattern Generator. The Journal of Neuroscience.
1356 Song, J., Ampatzis, K., Björnfors, E.R., and El Manira, A. (2016). Motor neurons control locomotor circuit
1357 function retrogradely via gap junctions. Nature 529, 399-402.
1358 Starich, T.A., Xu, J., Skerrett, I.M., Nicholson, B.J., and Shaw, J.E. (2009). Interactions between innexins
1359 UNC-7 and UNC-9 mediate electrical synapse specificity in the Caenorhabditis elegans locomotory
1360 nervous system. Neural Development 4, 16.
1361 Stiernagle, T. (2006). Maintenance of *C. elegans*. In Wormbook, T.C.e.R. Community, ed.
1362 Stirman, J., Crane, M., Husson, S.J., Wabnig, S., Schultheis, C., Gottschalk, A., and Lu, H. (2011). Real-time
1363 multimodal optical control of neurons and muscles in freely behaving Caenorhabditis elegans. Nature
1364 Methods 8, 153-159.
1365 Sulston, J., and Hodgkin, J. (1988). Methods. In The Nematode Caenorthabditis elegans, W.B. Wood, ed.
1366 (Cold Spring Harbor, NY: Cold Spring Harbor Laboratory Press).
1367 Turek, M., Lewandrowski, I., and Bringmann, H. (2013). An AP2 Transcription Factor Is Required for a
1368 Sleep-Active Neuron to Induce Sleep-like Quiescence in C. elegans. Current Biology 23, 2215-2223.
1369 Varshney, L.R., Chen, B.L., Paniagua, E., Hall, D.H., and Chklovskii, D.B. (2011). Structural Properties of
1370 the <italic>Caenorhabditis elegans</italic> Neuronal Network. PLoS Comput Biol 7, e1001066.

1371 Waggoner, L.E., Zhou, G.T., Schafer, R.W., and Schafer, W.R. (1998). Control of Alternative Behavioral
1372 States by Serotonin in Caenorhabditis elegans. Neuron 21, 203-214.
1373 Weeks, J.C. (1981). Neuronal basis of leech swimming: separation of swim initiation, pattern generation,
1374 and intersegmental coordination by selective lesions. Journal of Neurophysiology 45, 698-723.
1375 Wen, Q., Po, M.D., Hulme, E., Chen, S., Liu, X., Wai, S., Kwok, Gershow, M., Leifer, A.M., Butler, V.*, et al.*
1376 (2012). Proprioceptive Coupling within Motor Neurons Drives C. elegans Forward Locomotion. Neuron
1377 76.
1378 Wendler, G. (1974). The influence of proprioceptive feedback on Locust flight co-ordination. Journal of
1379 comparative physiology 88, 173-200.
1380 White, J., Southgate, E., Thomson, J., and Brenner, S. (1986). The Structure of the Nervous System of the
1381 Nematode Caenorhabditis elegans. Philosophical Transactions of the Royal Society of London B 314, 1-
1382 340.
1383 White, J.G., Southgate, E., Thomson, J.N., and Brenner, S. (1976). The Structure of the Ventral Nerve
1384 Cord of Caenorhabditis elegans. Philosophical Transactions of the Royal Society of London B, Biological
1385 Sciences 275, 327-348.
1386 Wicks, S., and Rankin, C. (1995). Integration of mechanosensory stimuli in Caenorhabditis elegans. The
1387 Journal of Neuroscience 15, 2434-2444.
1388 Xu, S., and Chisholm, A.D. (2016). Highly efficient optogenetic cell ablation in C. elegans using
1389 membrane-targeted miniSOG. 6, 21271.
1390 Yu, X., and Friesen, W.O. (2004). Entrainment of leech swimming activity by the ventral stretch receptor.
1391 Journal of Comparative Physiology A 190, 939-949.
1392 Yu, X., Nguyen, B., and Friesen, W.O. (1999). Sensory Feedback Can Coordinate the Swimming Activity of
1393 the Leech. The Journal of Neuroscience 19, 4634.

1394 Zhang, F., Wang, L.-P., Brauner, M., Liewald, J.F., Kay, K., Watzke, N., Wood, P.G., Bamberg, E., Nagel, G.,
1395 Gottschalk, A., and Deisseroth, K. (2007). Multimodal fast optical interrogation of neural circuitry.
1396 Nature 446, 633-639.
1397 Zhen, M., and Samuel, A. (2015). C. elegans locomotion: small circuits, complex functions. Current
1398 Opinion ini Neurobiology 33, 117-126.
1399 Zheng, M., Friesen, W.O., and Iwasaki, T. (2007). Systems-level modeling of neuronal circuits for leech
1400 swimming. J Comput Neurosci 22, 21-38.
1401 Zheng, Y., Brockie, P.J., Mellem, J.E., Madsen, D.M., and Maricq, A.V. (1999). Neuronal Control of
1402 Locomotion in C. elegans Is Modified by a Dominant Mutation in the GLR-1 Ionotropic Glutamate
1403 Receptor. Neuron 24, 347-361.

1404

**Figure 1. Overview of curvature analysis and models of rhythm generation**

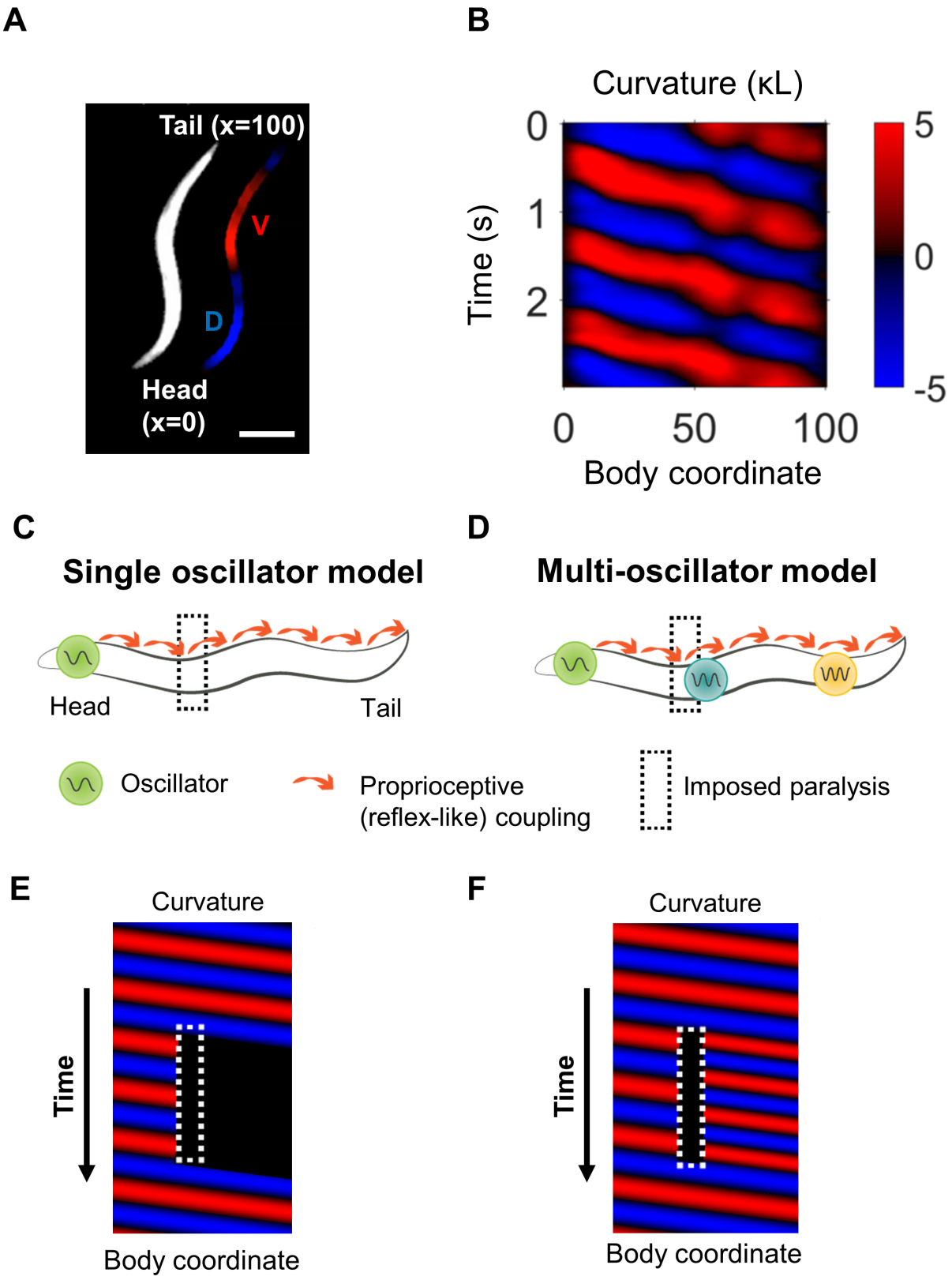

**Figure 2: Anterior undulation is not required for posterior undulation**

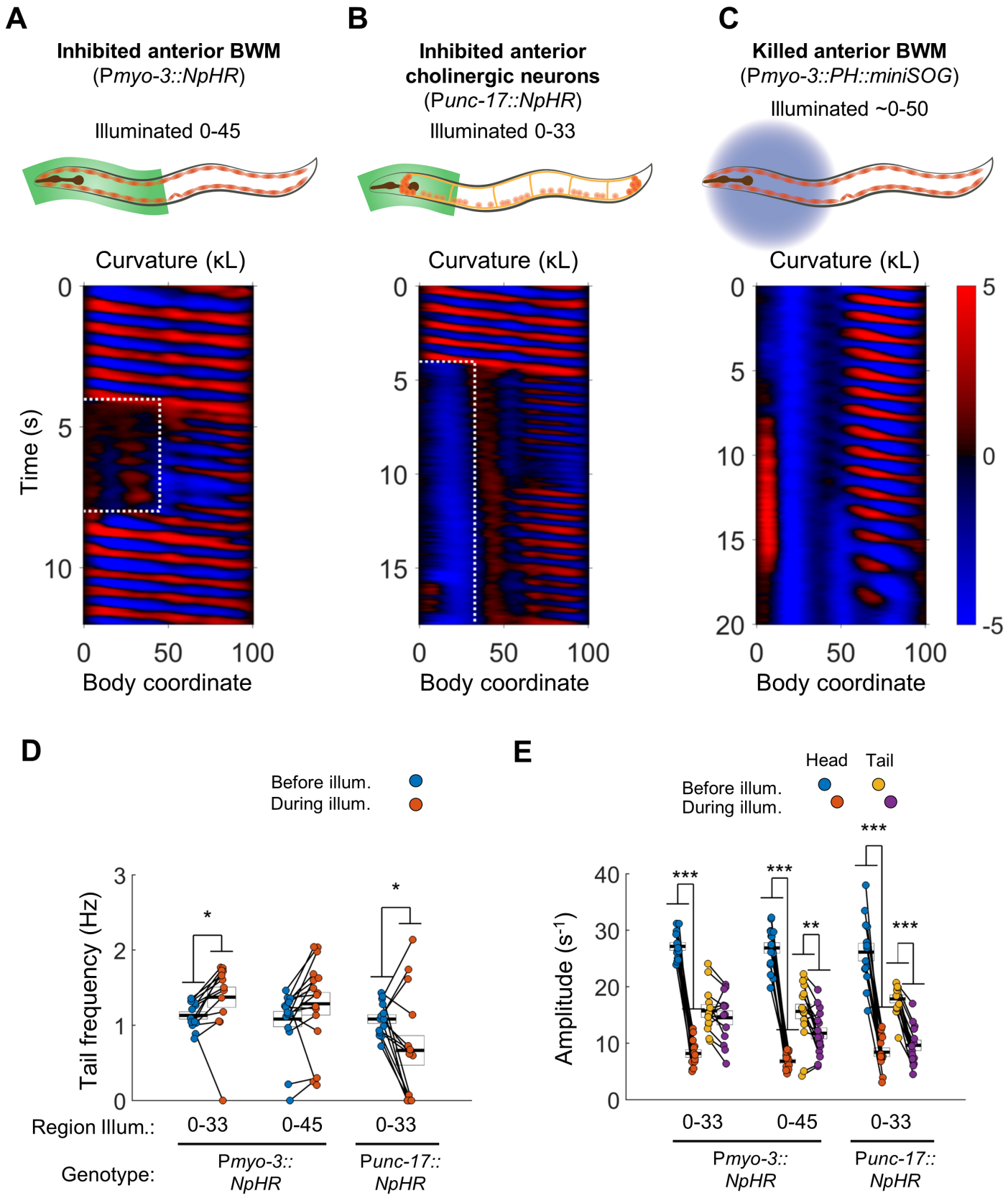

**Figure 3: Disruption of motor coupling in the neck de-synchronizes oscillations in the head and tail**

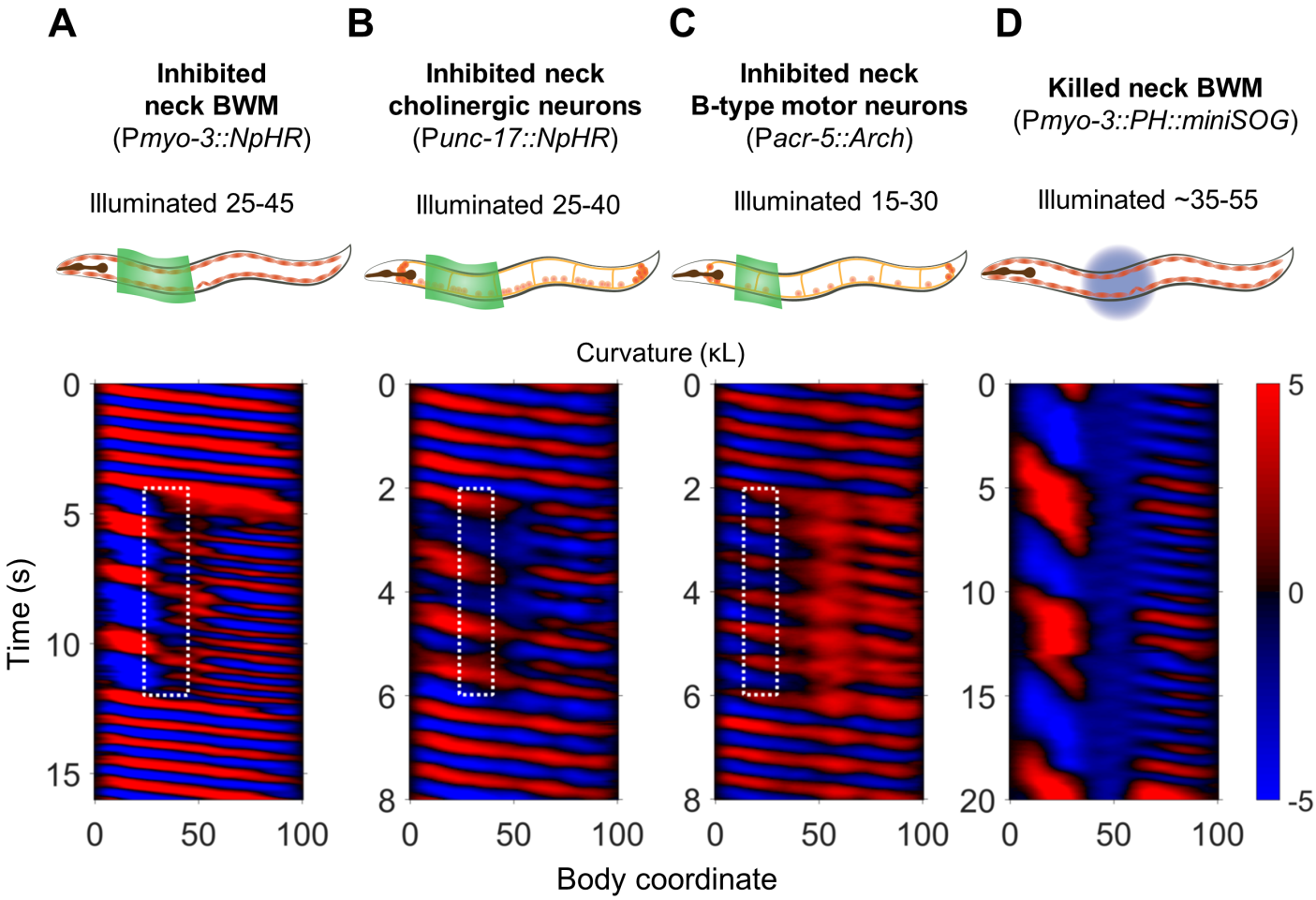


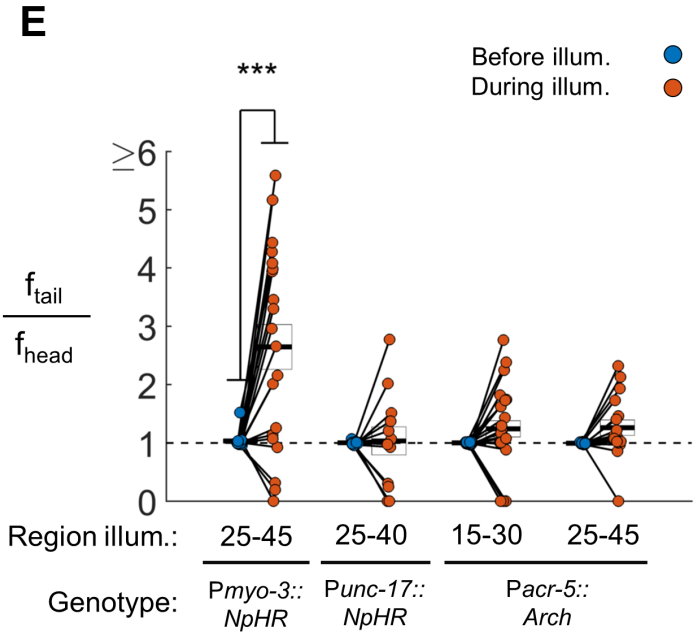


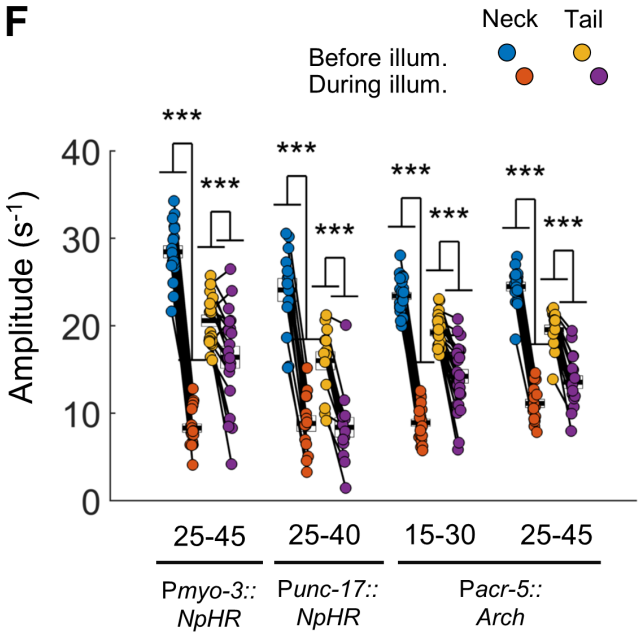

**Figure 4. VNC premotor interneurons, D-type motor neurons, and individual B-type motor neurons are not required for 2FU**

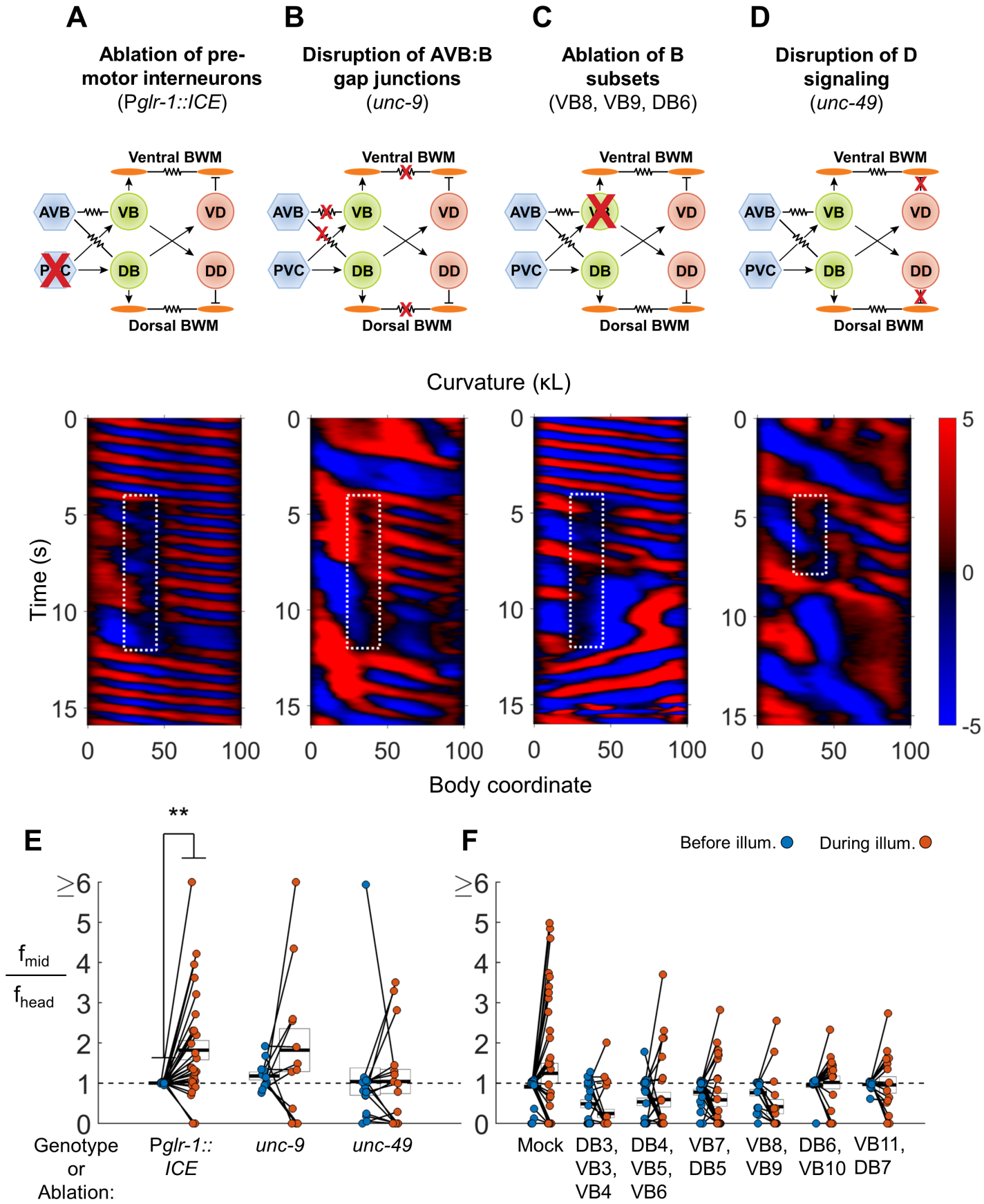

**Figure 5. B motor neurons are required for 2FU**

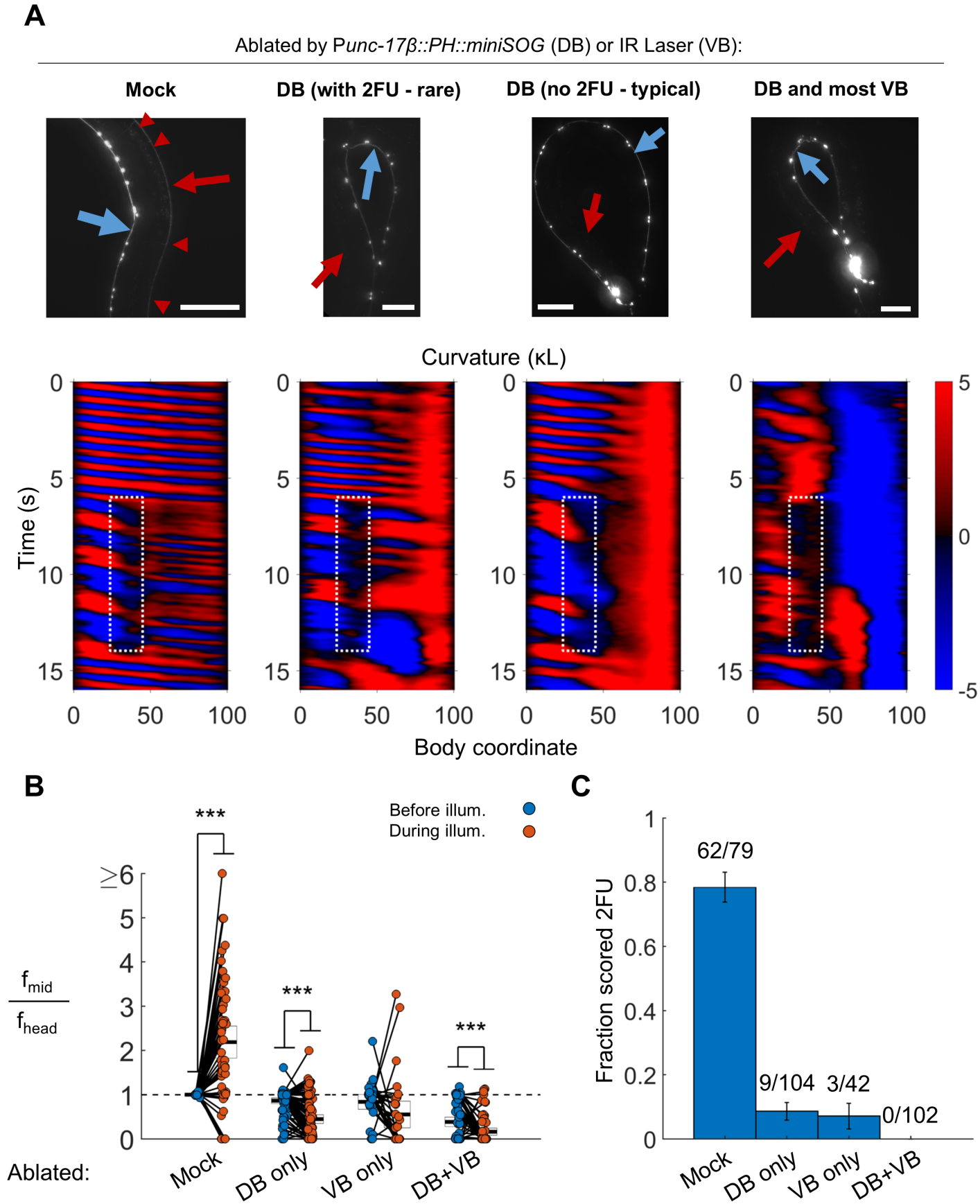

**Figure 6: Undulations generated in the tail after severing the dorsal and ventral nerve cords**

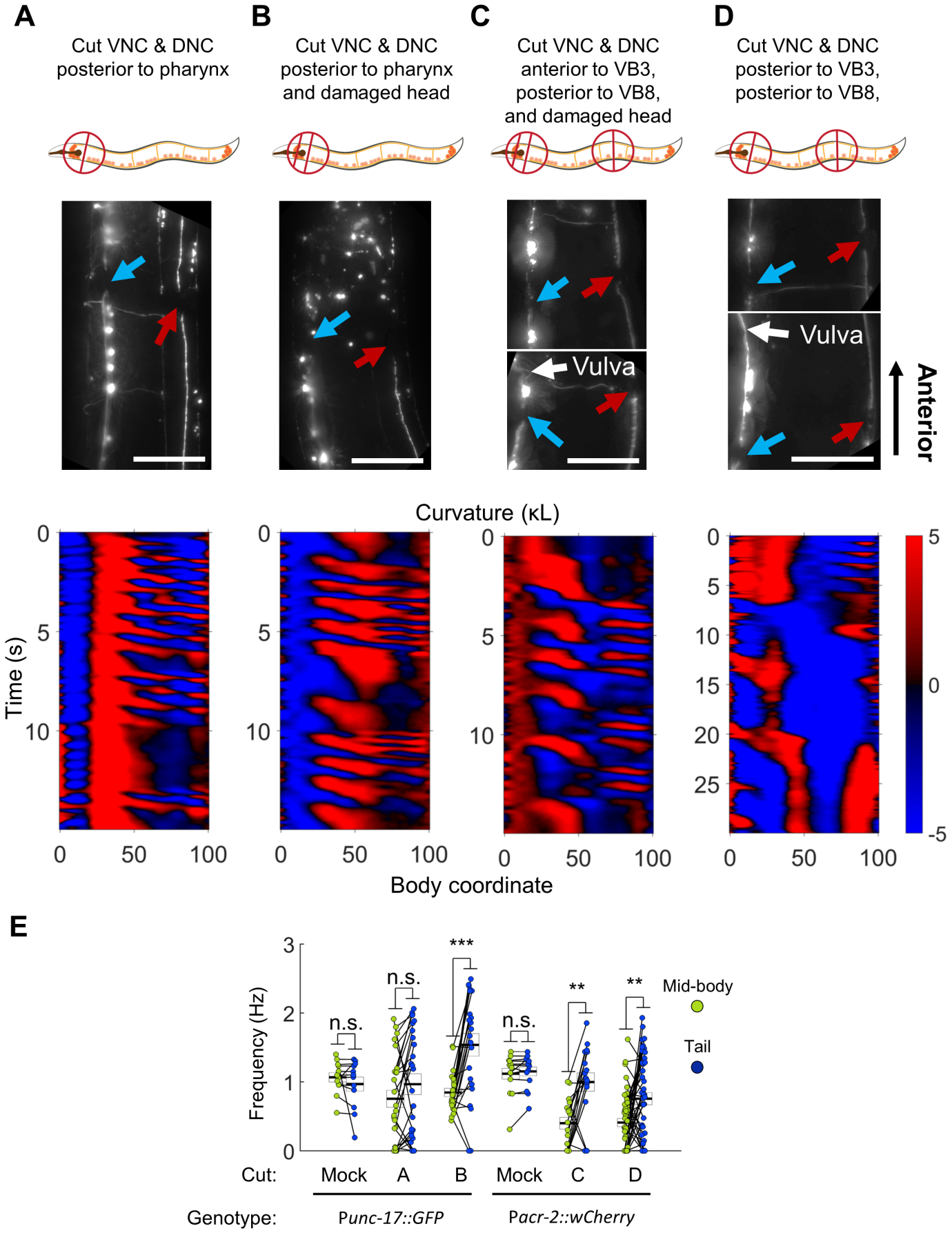

**Figure 7: Tail undulations after severing the VNC and DNC in various locations.**

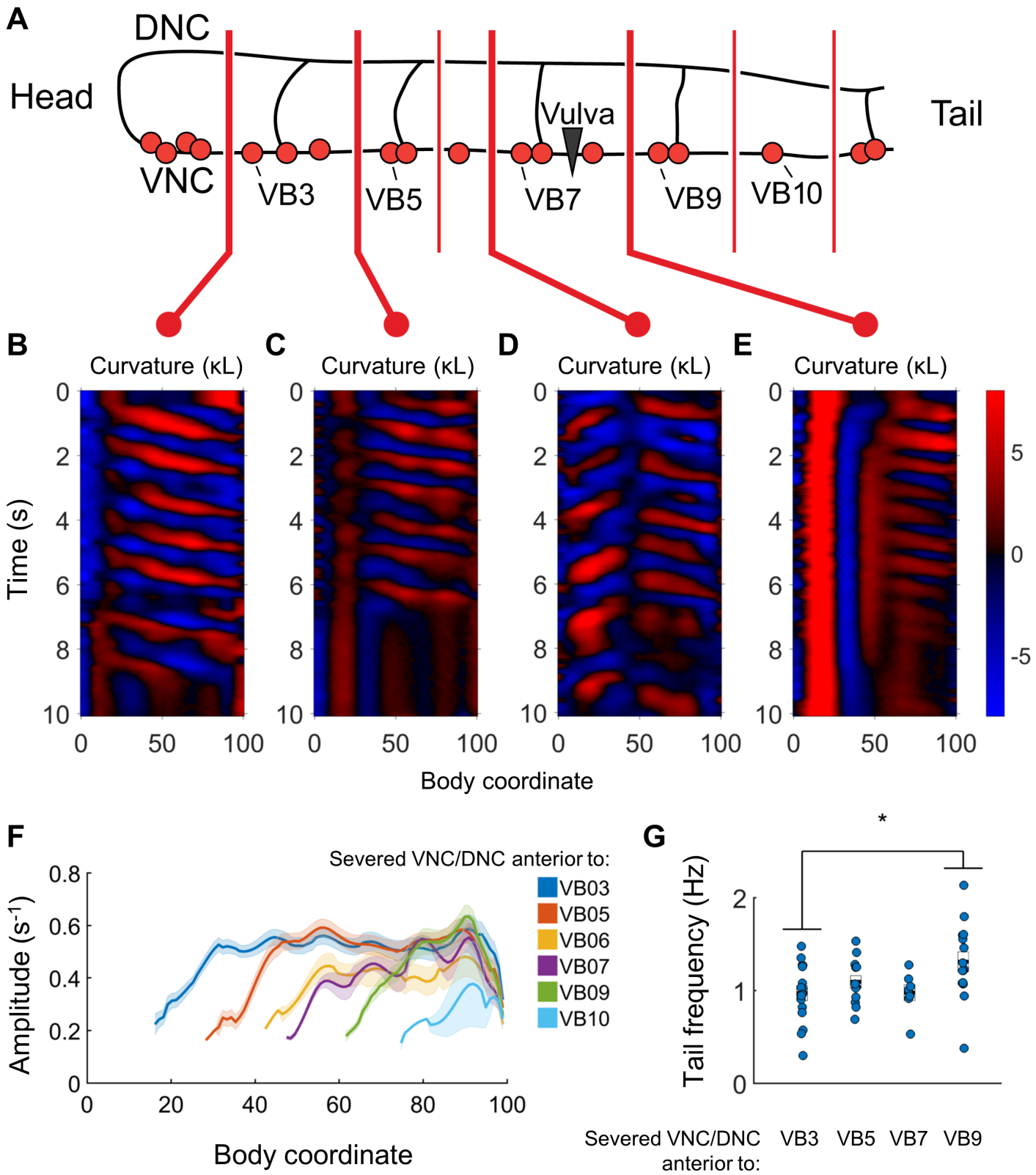

**Figure 8: Head undulation frequency can be entrained by mid-body rhythmic inhibition**

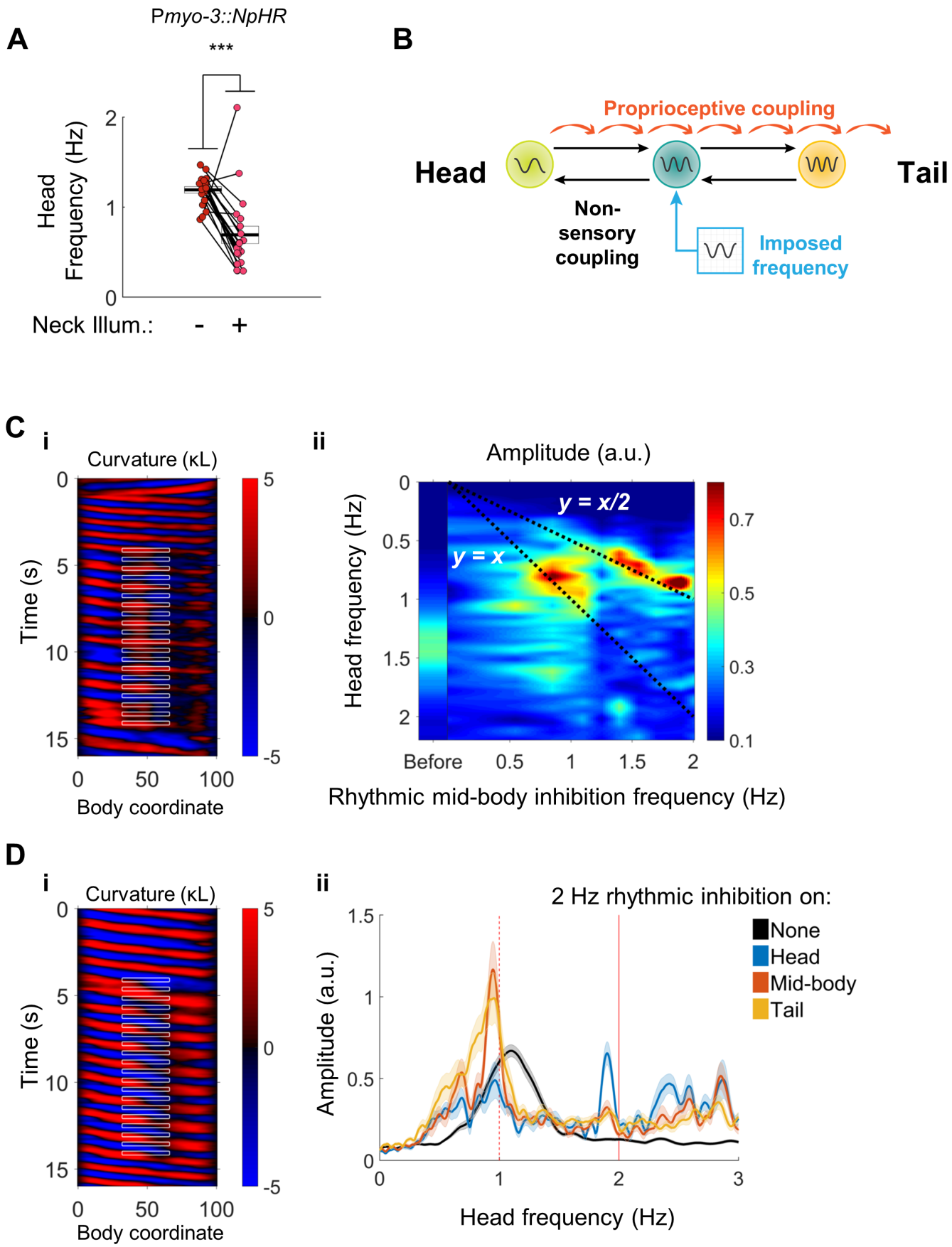

**Figure 9: Overview of forward locomotion**

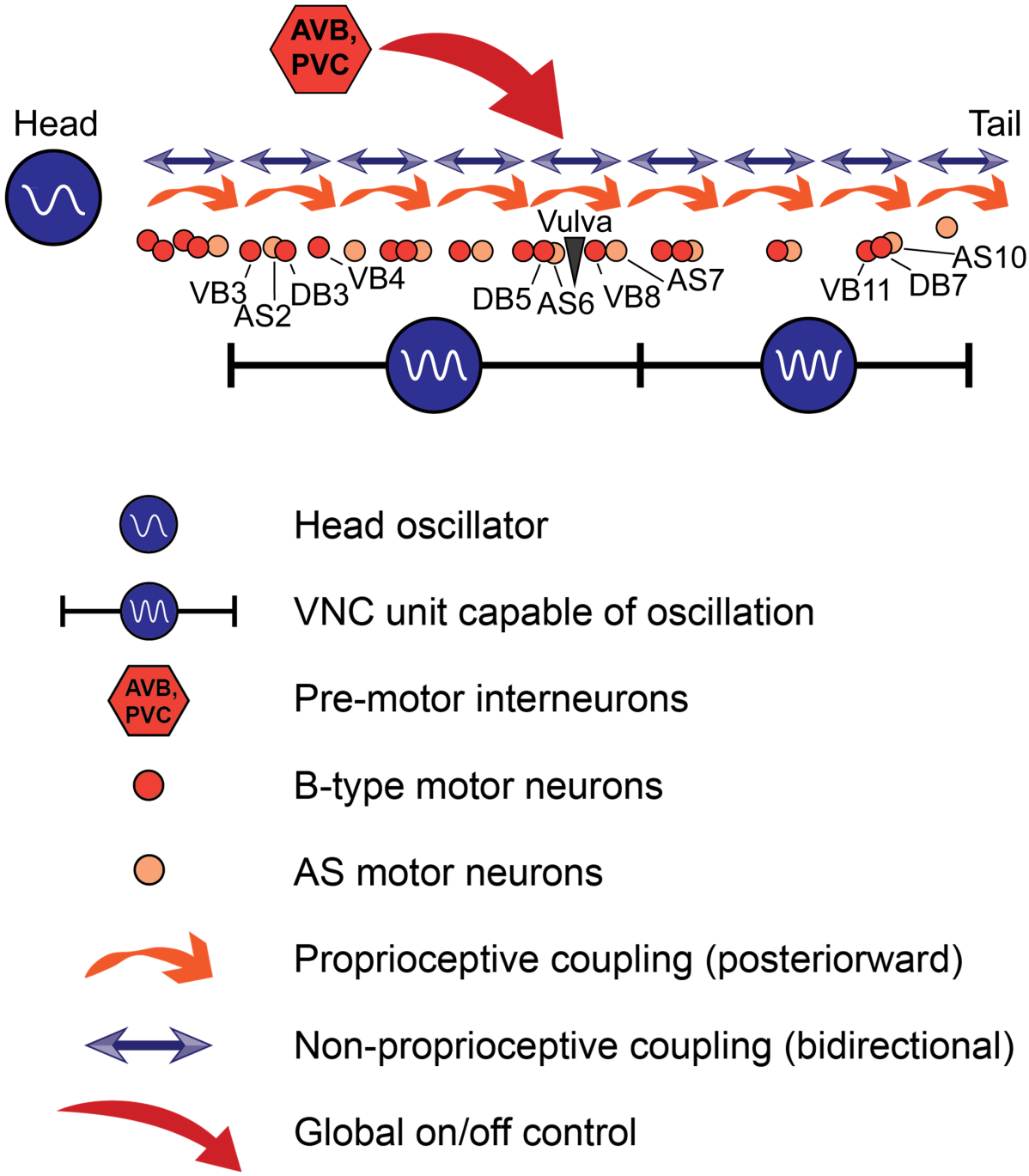

**Figure 2 Figure Supplement 1: Tail undulation after gross head lesioning**

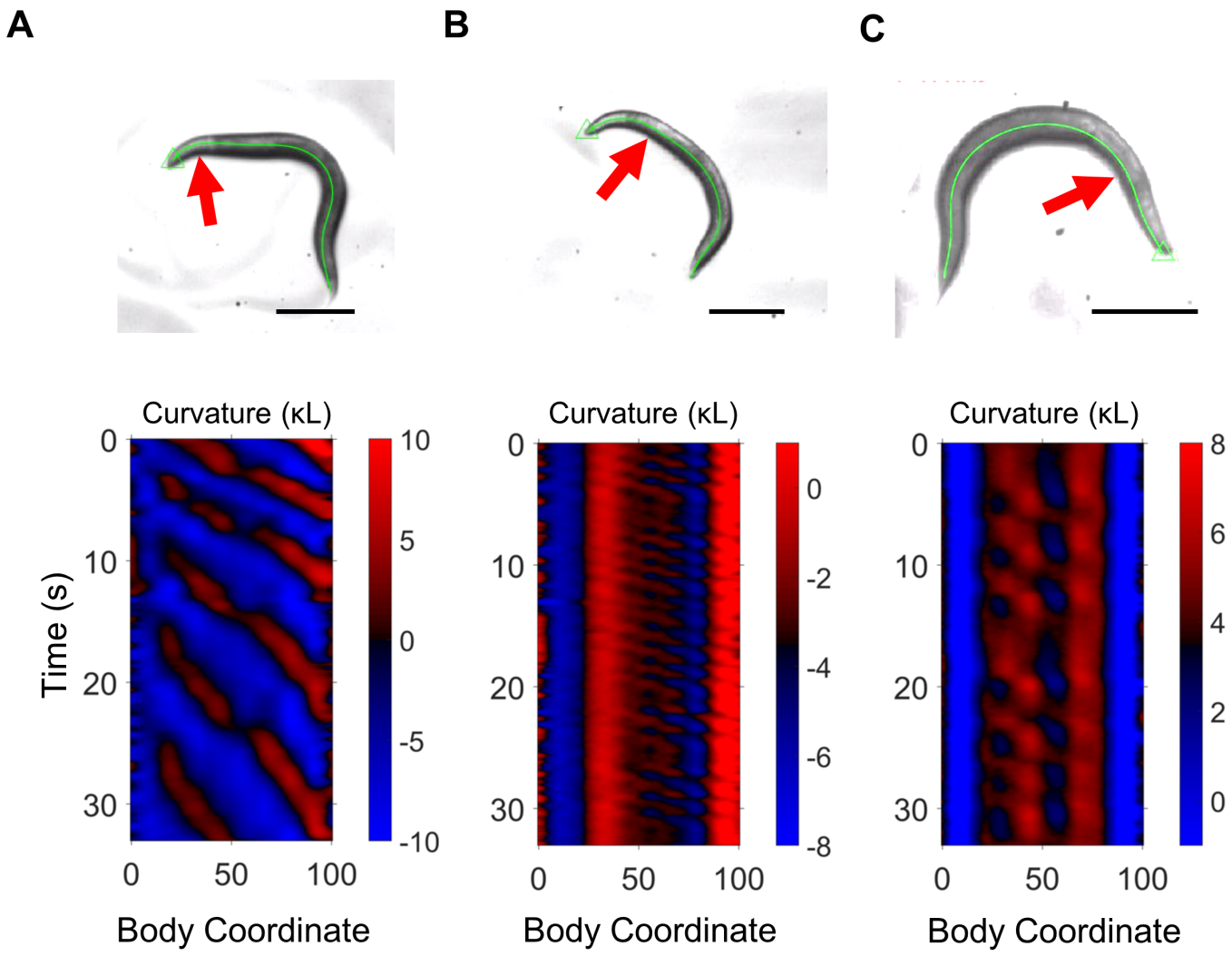

**Figure 3 Figure Supplement 1: Additional disruptions to motor coupling cause two-frequency undulation**

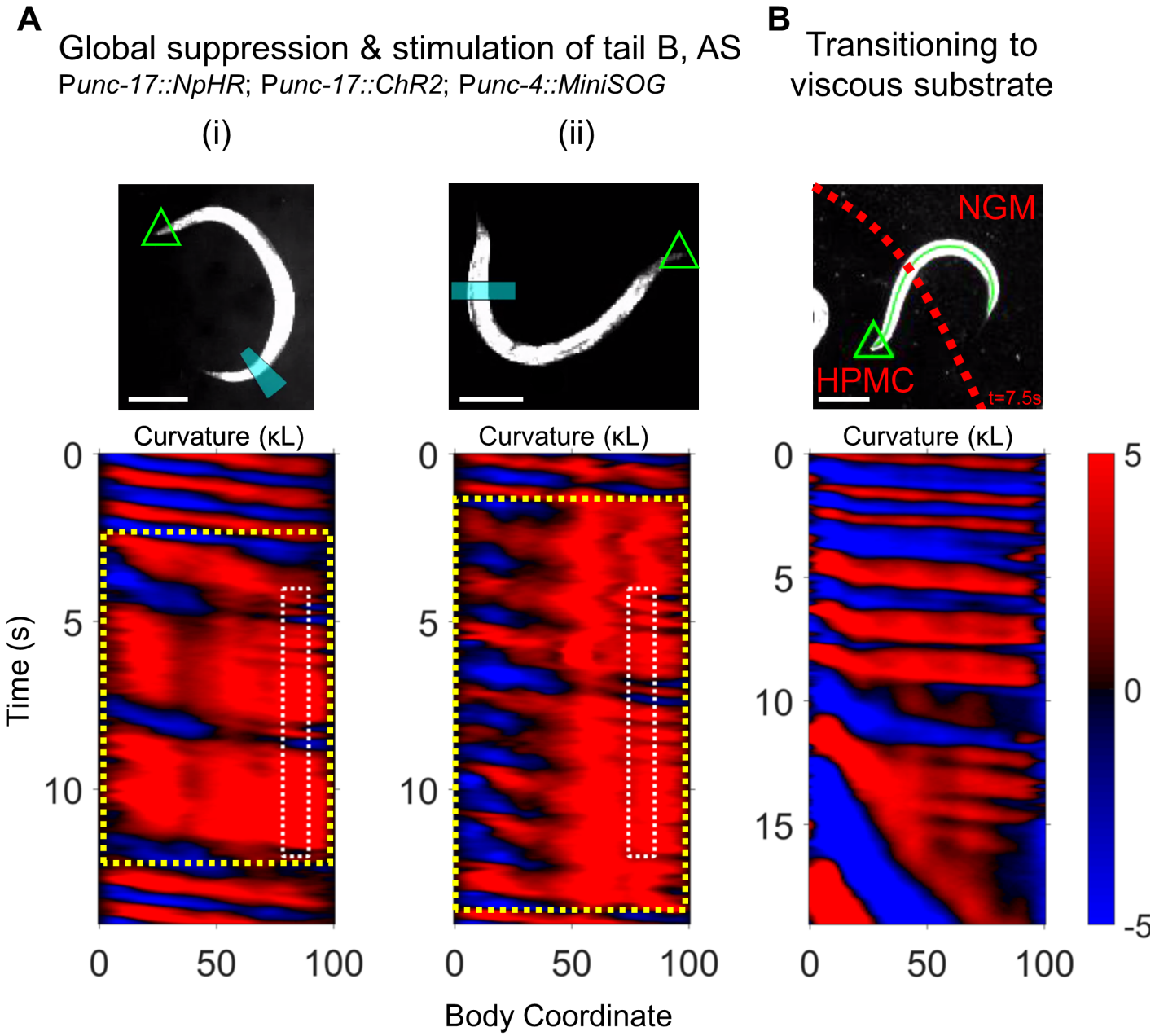

**Figure 4 Figure Supplement 1: VNC premotor interneurons and several VNC motor neuron classes are not required for de-synchronized oscillations**

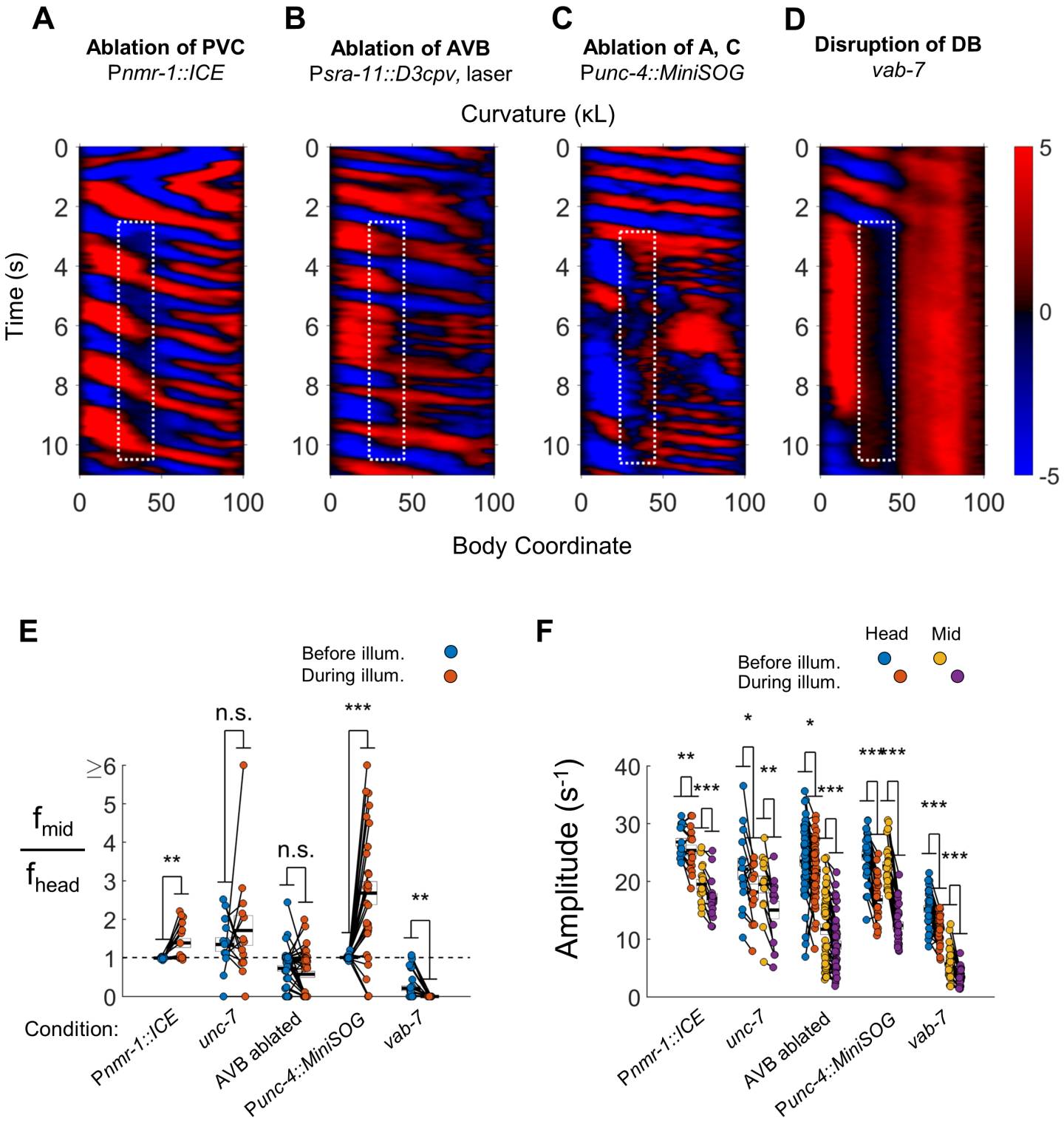

**Figure 4 Figure Supplement 2: Laser ablation of AVB**

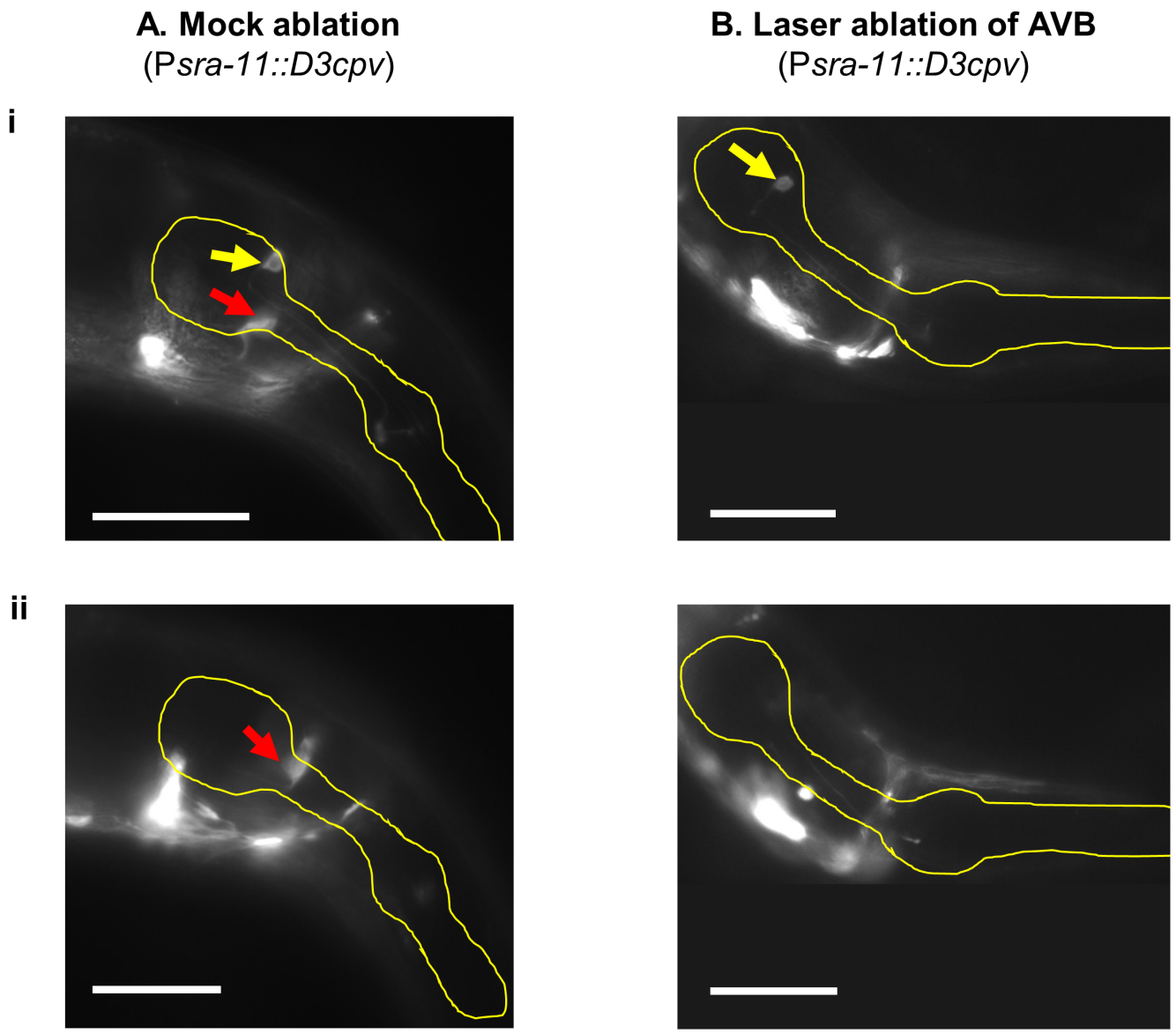

**Figure 4 Figure Supplement 3: Subsets of B-type motor neurons are not required for 2FU**

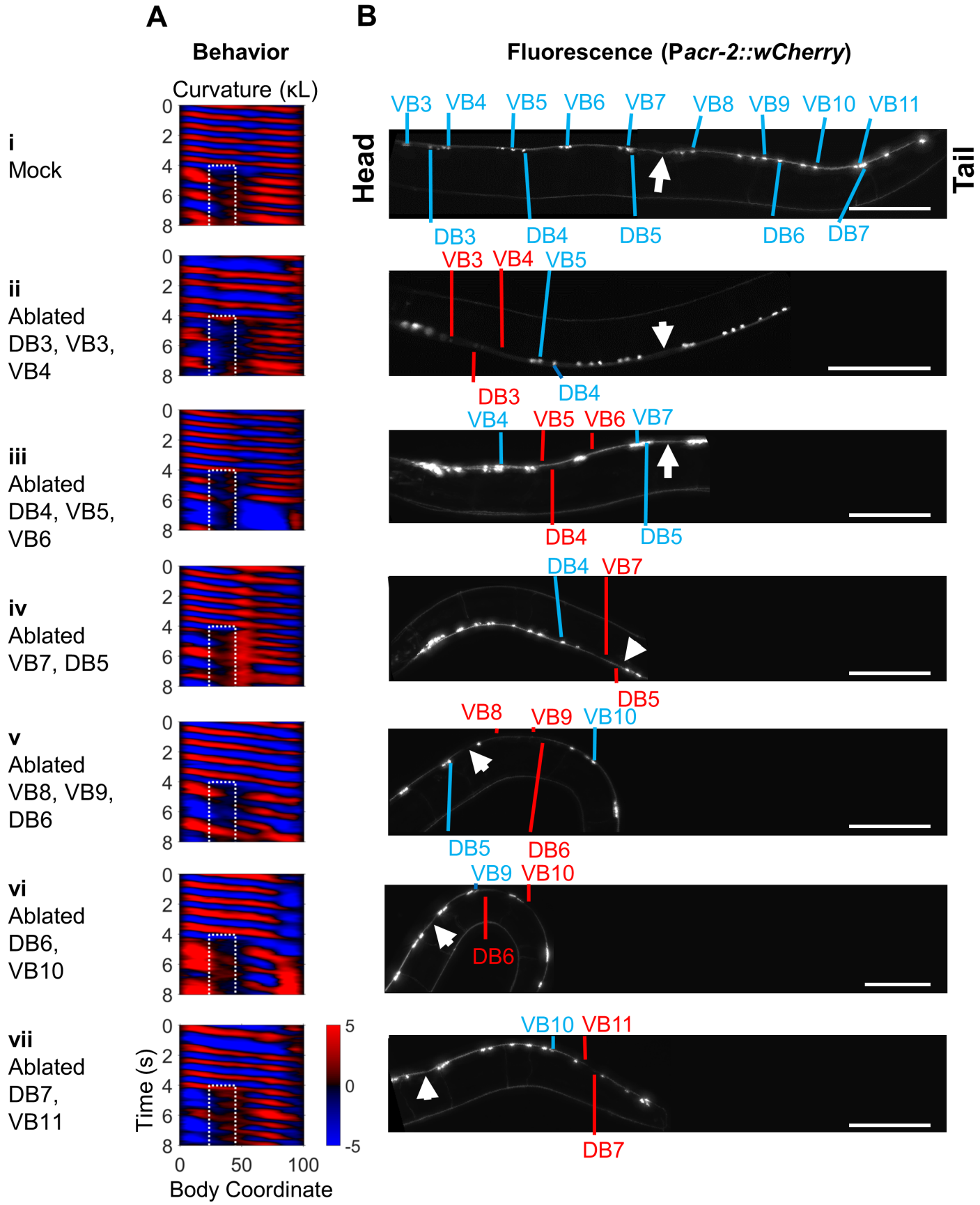

**Figure 4 Figure Supplement 4: B-type motor neurons posterior to the vulva are not required for 2FU**

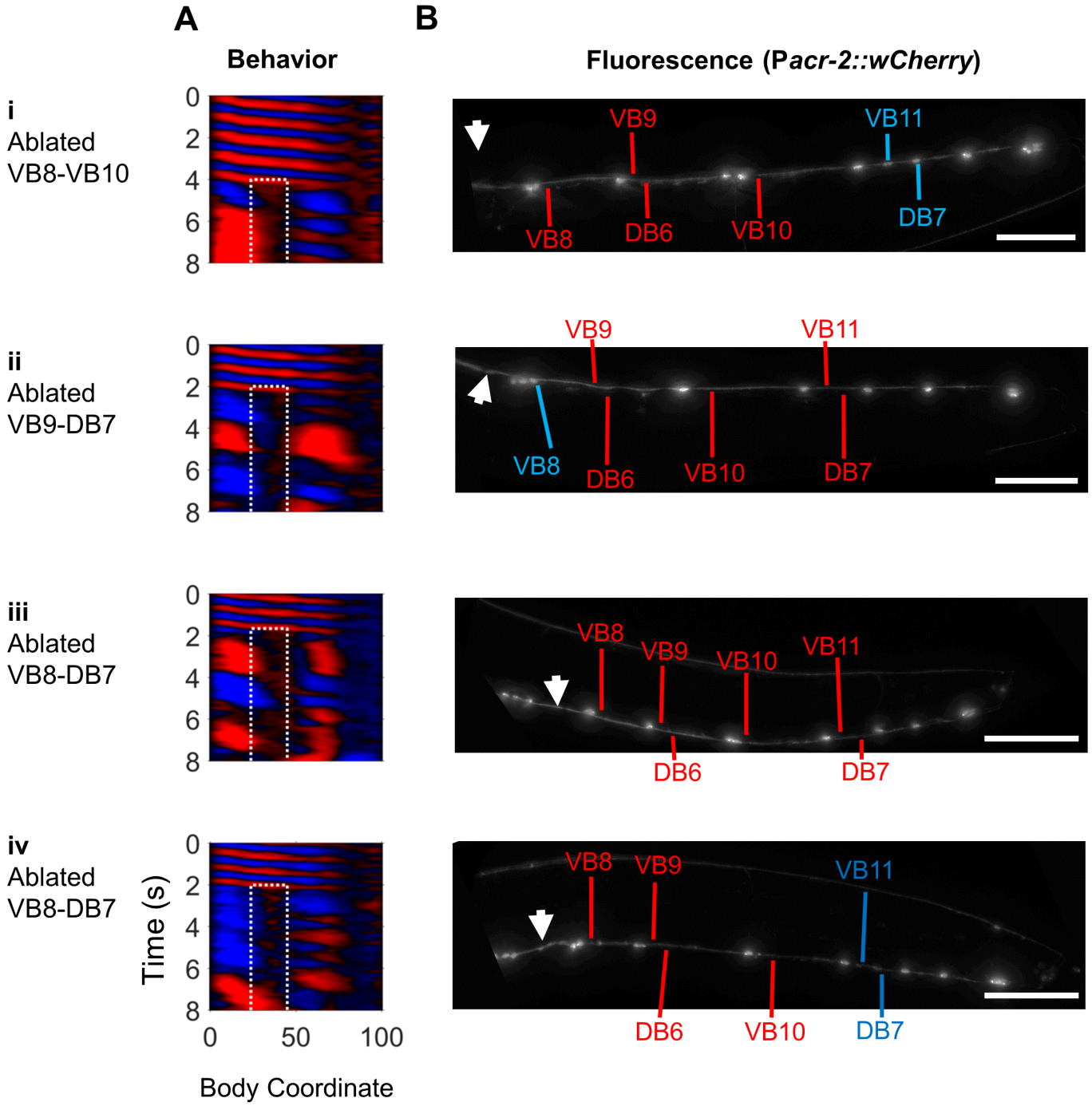

**Figure 4 Figure Supplement 5: 2FU may occur without neck muscle relaxation in strains with motor circuit disruptions**

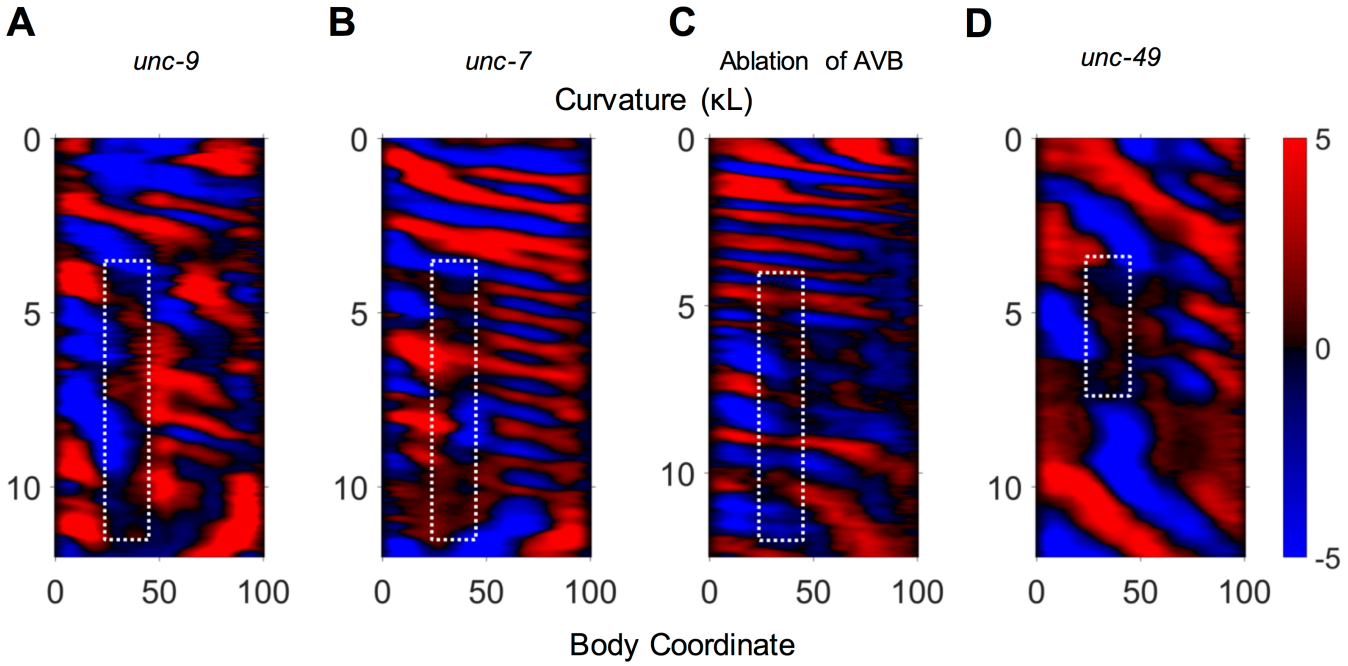

**Figure 5 Figure Supplement 1: Ablation of VB motor neurons**

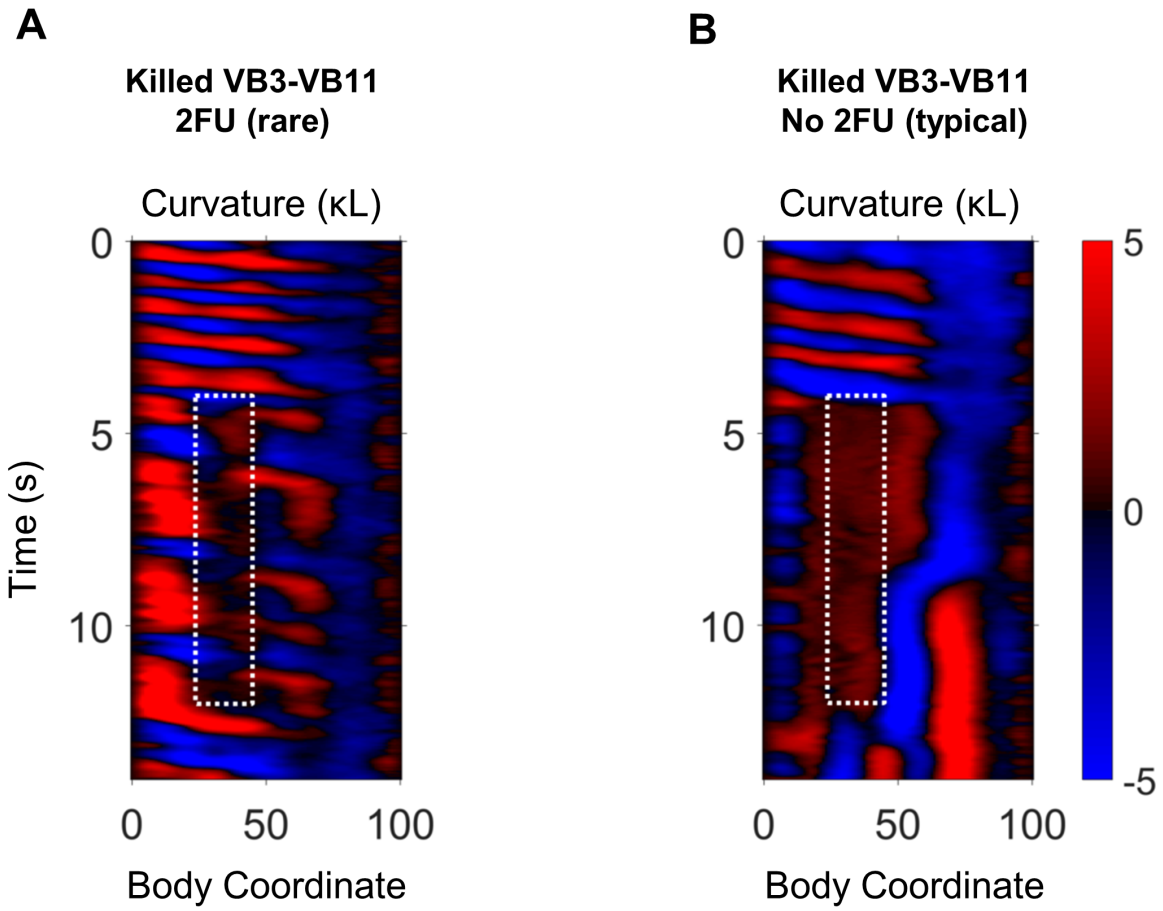

**Figure 6 Figure supplement 1: A motor neurons are not required for undulation after severing nerve cords**

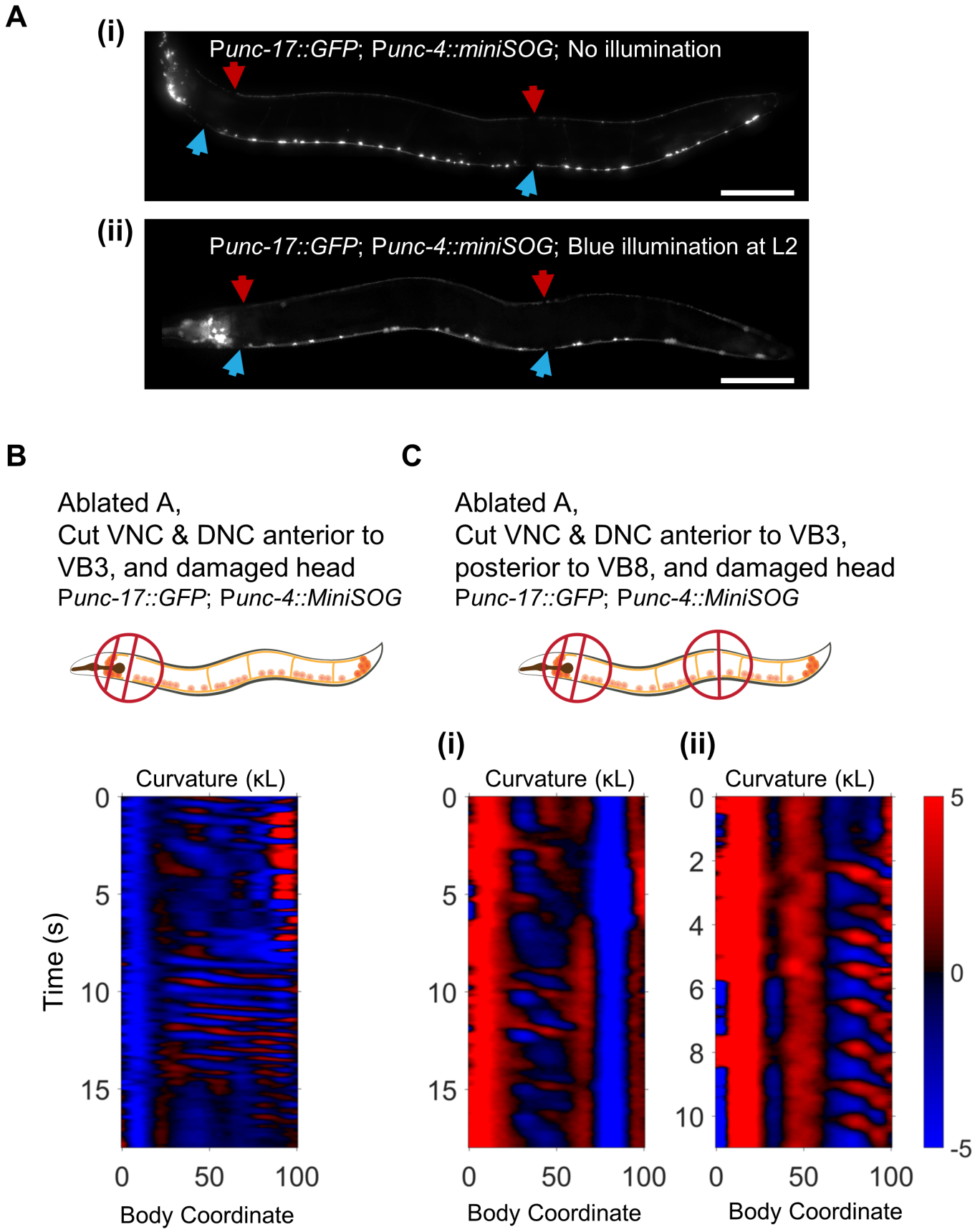

**Figure 6 Figure supplement 2:** **B motor neurons are required for undulation after severing nerve cords**

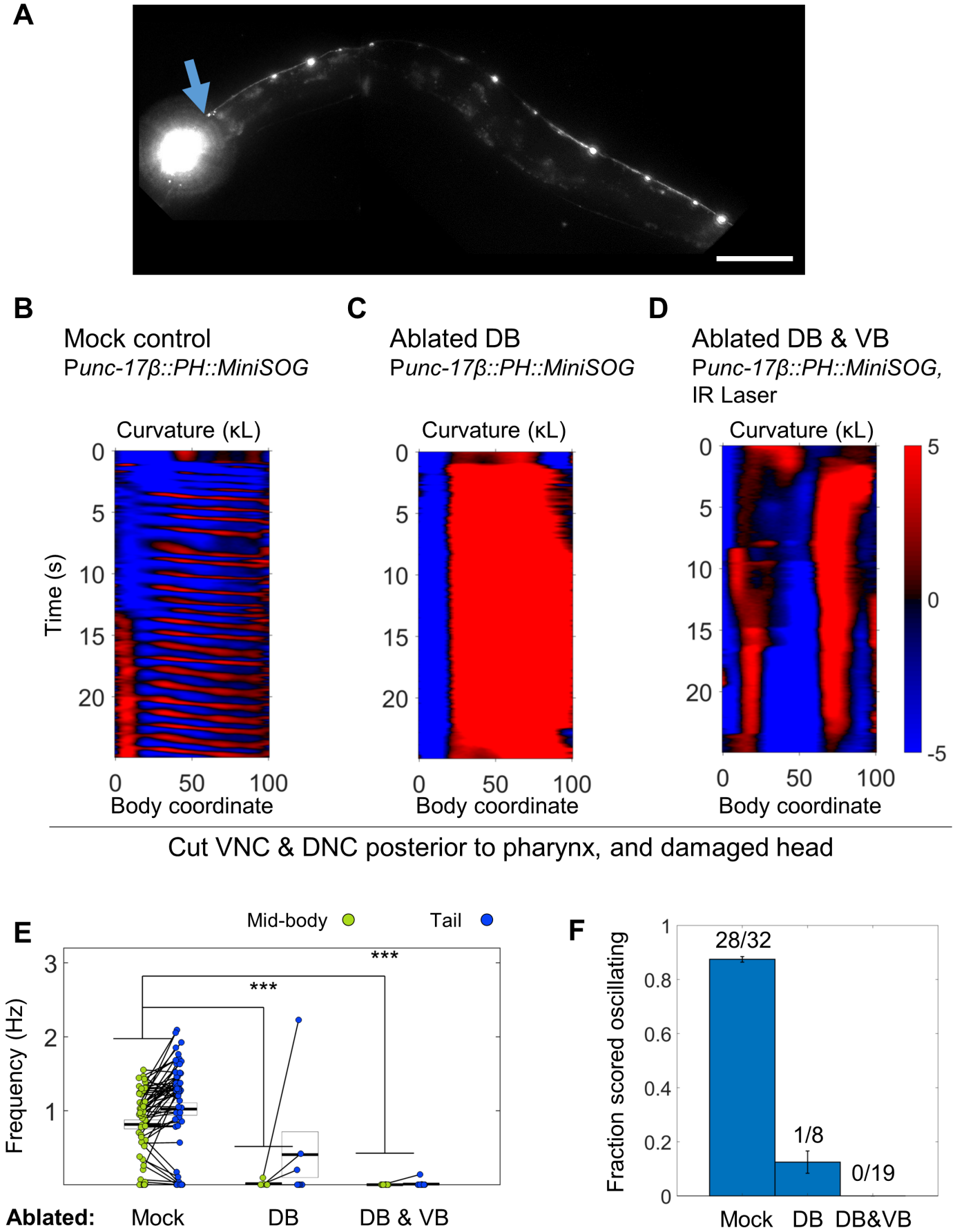
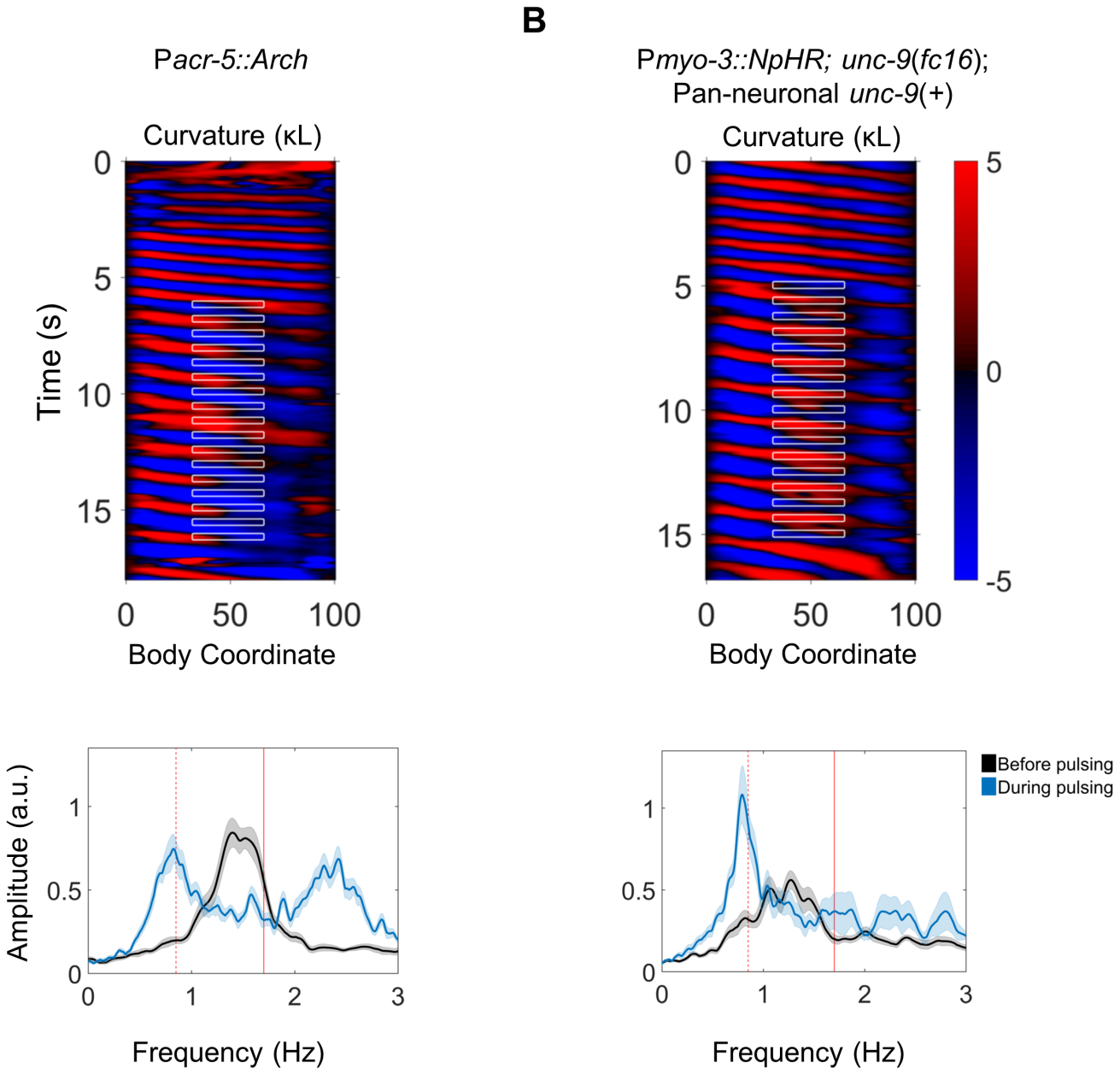
**Figure 8 Figure Supplement 1: VNC Cholinergic neurons mediate posterior-to-anterior entrainment**